Apollo 14 Very High Potassium Basalt Petrogenesis: Influence of Magma Chamber and Impact Processes

Sarah Roberts

Publication Date

15-04-2015

APOLLO 14 VERY HIGH POTASSIUM BASALT PETROGENESIS: INFLUENCE OF MAGMA CHAMBER AND IMPACT PROCESSES

A Thesis

Submitted to the Graduate School

of the University of Notre Dame

in Partial Fulfillment of the Requirements

for the Degree of

Master of Science

in Earth Sciences

by

Sarah Elizabeth Roberts

_____

Clive Neal, Director

Graduate Program in Civil and Environmental Engineering and Earth Sciences

Notre Dame, Indiana

April 2015

This is dedicated to Lin Li at IUPUI for introducing

me to planetary geology.

CONTENTS

FIGURES

ACKNOWLEDGMENTS

Many thanks to Clive Neal for his patience with me, and to Karl Cronberger, Pat Donohue, Amy Fagan, Jeremy Fein, Tony Simonetti, Andy Barth, Mollie Dash, Julia Hennion, and Bonnie Prestin.

INTRODUCTION

Lunar mare basalts provide a means to study the composition of at least the upper mantle of the Moon (e.g., Shervais et al., 1985b). As windows into the lunar interior, they have indirectly recorded lunar thermal evolution, and investigating the petrogenesis of these basalts is also a study into the early history and chemical differentiation of the Moon. Chemical variations among the suites of rocks collected from the Apollo missions demonstrate chemical heterogeneity in the mantle source regions (e.g., Neal and Taylor, 1992). However, various processes that affected these basalts after the parent magmas separated from the source region can complicate the study of source region composition. This paper uses microanalytical techniques to examine the petrogenesis of the Very High Potassium (VHK; Shervais et al., 1985b) basalts described from samples returned from the Apollo 14 landing site.

The Apollo 14 mission in 1971 landed in the Fra Mauro region of the Moon, which is believed to be impact ejecta from the creation of the Imbrium basin (Sutton et al., 1972) (Figure 1). A total of 42.3 kg of samples were returned by the mission many of the rock samples comprising complex breccias that contain clasts of older breccias, basalts, and highlands lithologies. These complex breccias yielded two previously uncollected types of basalts, high-Al with >11 wt.% Al_2O_3 (Ridley, 1975;

Shervais et al., 1985a; Neal and Taylor, 1992), and a Very High Potassium (VHK – K_2O >0.5 wt.%) (Shervais et al., 1985b).

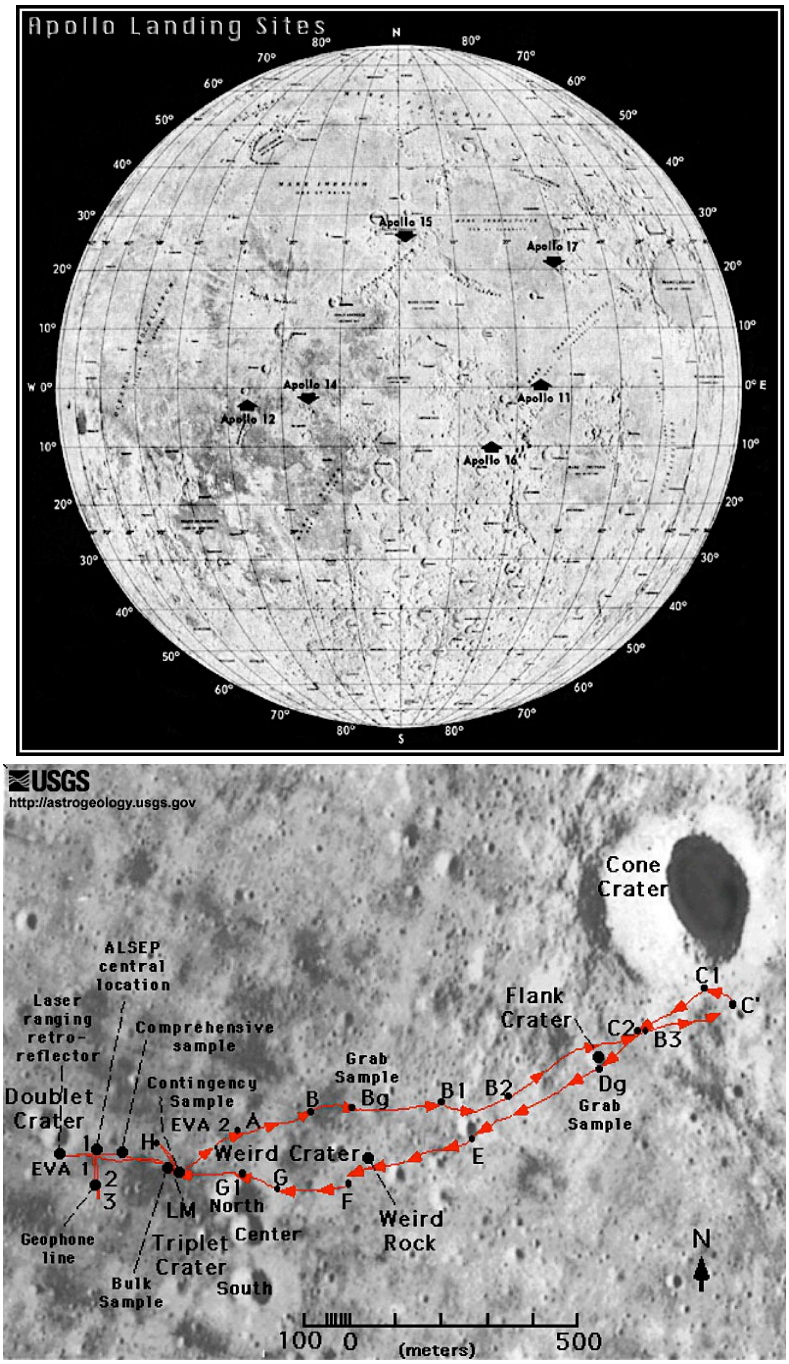

Figure 1. Apollo 14 landing site (top) and traverse of the Apollo 14 mission (bottom). VHK basalts were collected 80m North, NorthWest of the lunar model. Images taken from *https://www.hq.nasa.gov/alsj/TraverseMapsEarth.html* and *http://astropedia.astrogeology.usgs.gov/download/Moon/Apollo/Traverse/AP14_traverseL.jpg*

Warner et al. (1980) described four mare basalts from the Apollo 14 coarse-fines collection and noted among them sample 14168,38. It contains abundant interstitial K-feldspar and K-Si-rich glass distributed throughout the sample, resulting in an unusually high K_2O content of 0.57 wt.%. Five years later, Shervais et al. (1985b) reinvestigated 14168,38 along with five clasts from breccia 14305 proposing the classification Very High Potassium (VHK) and the type characterization of these basalts as K_2O > 0.5 wt.%, K_2O/Na_2O >1, and K/La ratios between 500 and 1300. The five VHK basalt samples had major element compositions nearly identical to high-Al basalts with the exception of elevated abundances of K_2O and Ba. The VHK basalts were described as medium to coarse-grained rocks with K-feldspar found within mesostasis material in intersertal areas. The random nature of the distribution of the glass and the variations in texture between the samples was attributed to different cooling rates and different positions within a single lava flow.

The enrichment of K that distinguishes the VHK basalts from other mare basalt has proved difficult in constructing a petrogenetic model for the VHK basalts and identifying the source of the enrichment. Using whole rock data of six VHK mare basalt samples, five clasts from breccia 14305 and sample 14168,38, Shervais et al. (1985b) hypothesized the formation of VHK basalts through the partial assimilation of granite by a parental high-Al mare basaltic magma. Goodrich et al. (1986) discovered two more VHK basalts in breccia 14304 with notably lower K_2O (~0.33 wt.% in each) and lower K/La ratios of between 580 and 700, suggesting a transitional composition between VHK and Apollo 14 high-Al basalts. The lower

K_2O abundances along with the coincidence of breccia 14305 and 14304 having been collected in the same weigh bag suggested that all of the VHK basalt samples were part of the same flow and compositional variations were due to modal heterogeneity. Goodrich et al. (1986) proposed an additional hypothesis for the formation of VHK basalts through the partial melting of a metasomatized source enriched in K, Rb, and Ba, but otherwise similar to a high-Al basalt source.

Shih et al. (1986) reported Rb-Sr, K-Ar, and Sm-Nd isotopic values on two of the previously identified VHK basalts, 14305,304, and 14168,39 (Shih et al., 1986). The ages derived from these data indicate formation between 3.83-3.94 Ga. The Sm-Nd isotopic whole rock data emphasized the similarities between VHK basalts and high-Al basalts showing that they are similar in age and chemistry with the exception of K and Rb abundances. Because of this relationship, Shih et al. (1986) concluded that both basalt types were produced by partial melting of similar source regions. Considering the Sm and Nd isotopic data, Shih et al. (1986) also suggested that the high abundances of K and Rb could be produced by the assimilation of granitic wall rocks by the high-Al basaltic magma during ascent.

With the discovery of five new VHK basalt samples in 1988 from breccia 14303, Neal et al. (1988) used whole rock data to construct an assimilation and fractional crystallization (AFC; Depaolo, 1981) model that encompassed all known VHK basalt samples. VHK basalt samples from breccia 14304 and 14305 were produced by assimilation of granite by a primitive high-Al basalt magma undergoing fractional crystallization. Samples from breccia 14303 require a more evolved high-Al basalt parental magma with KREEP replacing granite as the assimilant during the

AFC process. With two different sources now needed for VHK basalt generation, VHK basalts were now linked to at least two different lava flows from two different eruptive events. Neal et al. (1988) concluded that the general crystallization path for the VHK basalts was identical to that proposed for high-Al basalts, with the enrichment of alkali elements (e.g., K, Rb, Ba) relative to normal high-Al basalt compositions being derived from from the granitic assimilant.

In a second study the following year, Neal et al (1989a,b) analyzed seven new VHK basalts from breccias 14303 and 14304 and identified the K-rich glass as the composition of the residual magma. The new data were similarly modeled by AFC (Neal et al., 1988) but required 3 parental high-Al basalts assimilating three distinct granite assimilant compositions. At least three VHK basalt eruptions forming at least three distinct flow units were now necessary to explain the new data.

The petrogenetic models formulated for the VHK basalts all consider the similarities VHKs have to high-Al basalts and involve high-Al parental magmas. However, none of these models have considered the possibility that VHK basalts could be impact melts, which traditionally can be investigated .by examining the content of high siderophile elements (HSEs), which are elevated in meteorites and asteroids. Melt rocks with HSE abundances >3 x 10-4 those of chondritic meteorites are considered to have been contaminated by the impactor and are not considered pristine (e.g., Warren and Wasson, 1980; Warren, 1993 and references therein). At least one sample contains elevated abundances of highly siderophile elements (HSE) (14303,277 - 3.9 ppb Ir, 2.7 ppb Au; Neal et al., 1988). Determining the pristine nature of lunar basalts by HSE analysis is unfavorable, especially for small basalt

clasts in breccias, as the sample is destroyed, and a small piece of adhering breccia matrix in the whole-rock aliquot can give a "false positive" result. Quantitative textural analysis using crystal size distributions (Cashman and Marsh, 1988; Marsh, 1988, 1998; Higgins, 2000, 2010) has been shown to be an effective alternative in distinguishing pristine mare basalts from impact melts by comparing the number of crystals and crystal size to the area of the sample displayed in a given thin section (Hui et al., 2011; Fagan et al., 2013; Neal et al., 2015).

Prior to 2013, all research on the petrogenesis of VHK basalts had been conducted using whole rock data. As an analytical method, whole rock chemistry averages all of the processes that have affected a sample, erasing valuable spatial and chronological information. For this study, we are revisiting VHK basalt samples using micro-analytical techniques, plagioclase crystal size distributions (CSDs), and elemental maps obtained from thin sections. Major and trace element abundances measured in situ by electron probe microanalysis (EPMA) and Laser Ablation ICP-MS (LA-ICP-MS), respectively, reveal relationships between high-Al and VHK basalts. Here we provide additional clues into the distribution of K within the samples and present a new hypothesis for the petrogenesis of VHK basalts.

SAMPLES/PETROGRAPHY

The VHK basalts are represented by one regolith fragment, 14168,38, and as clasts in three breccias: 14303, 14304, and 14305. Breccia 14303 was originally part of breccia 14304 and breccias 14304 and 14305 were collected in the same weigh bag (Meyer, 2007; Goodrich et al., 1986). Thirteen VHK basalt samples were analyzed from all three breccias for this study: two clasts from breccia 14303, seven clasts from breccia 14304, and four clasts from breccia 14305. Sample 14304,221 is also represented by 2 additional probe mounts, 299 and 326. In the descriptions below, each sample is represented by thin section numbers. Corresponding whole-rock sample numbers, where applicable, are given in Table 1.

TABLE 1

NUMBERING OF VHK BASALT SAMPLES

Breccia	**Whole-Rock Sample No.**	**Probe Mount No.**
14303	244	245
14303	318	328
14304	168	169
14304	176	177
14304	148	187
14304	152	189
14304	180	203
14304	221	221,299,326
14304	243	324
14305	373	380
14305	384	383
14305	382	388
14305	390	393

The VHK basalts show a variety of textures and characteristics ranging from granulated to coarse grained. Euhedral to subhedral plagioclase crystals from 0.25 to 1mm long are common in predominantly ophitic to subophitic textures. Olivine either is not present, present as cores to pyroxene crystals, and/or as individual grains. Interstitial K-rich glass is found in varying abundance, with K-feldspar being an interstitial phase. Brief petrographic descriptions are given here, as each sample has been previously described in detail.

14303, 245: This medium-grained ophitic-textured groundmass sample contains tabular plagioclase crystals up to 0.5mm (Figure 2a). Two corroded grains of olivine are present and olivine inclusions are found in some of the larger plagioclase crystals (Neal et al., 1988).

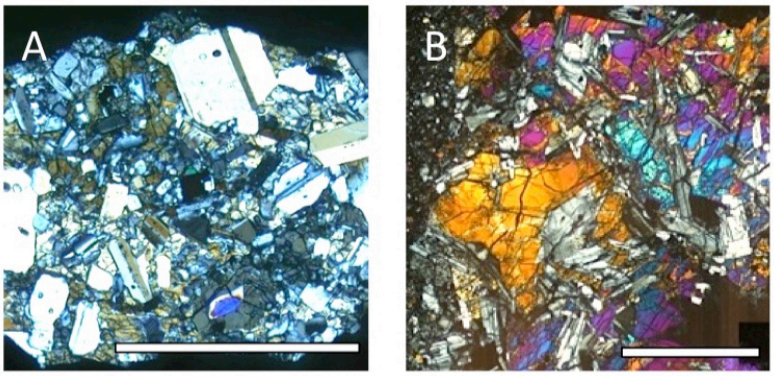

Figure 2. Photomicrographs of VHK basalt clasts from breccia 14303. Scale bar represents 1mm. (a)14303,245 (b) 14303,328

14303, 328: This coarse-grained, ophitic basalt was originally described by Neal et al. (1989a) (Figure 2b). Plagioclase crystals are up to 1.5 mm in length and corroded olivine crystals exist in the cores of pyroxene and as individual grains. Interstitial glass is present and breccia matrix is attached to the basalt clast in the thin section studied.

14304, 169: This inequigranular to granular basalt has large plagioclase phenocrysts approximately 1mm long and interstitial pyroxenes up to 0.5mm long (Neal et al., 1989a) (Figure 3a). No olivine is found within this sample. Apatite is noted as a minor interstitial phase (≤0.1 mm). Three fragments of this sample are

present in the thin section. Adhering breccia matrix is present in all three fragments.

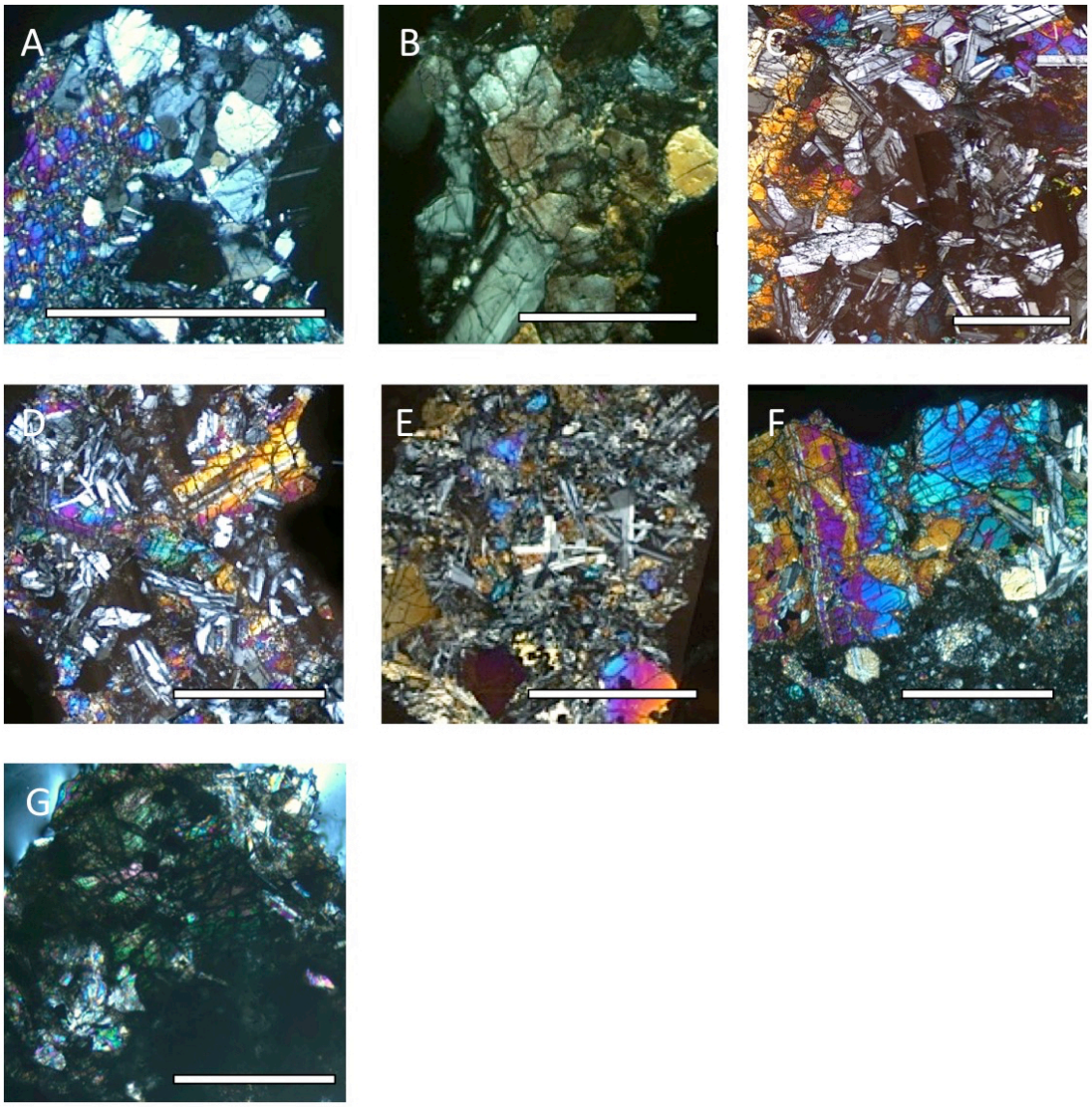

Figure 3. Photomicrographs of VHK basalts from breccia 14304 in cross polarized light. Scale bar represents 1mm. (a) 14304,169. (b) 14304,177. (c) 14304,187. (d) 14304,189. (e) 14304,203. (f) 14304,221. (g) 14304,324.

14304, 177: This noritic basalt is coarse-grained with an interlocking texture of pyroxene and plagioclase (Neal et al., 1989a) (Figure 3b). Wormy exsolution textures are found in some of the pyroxenes. Interstitial glass is abundant and apatite is a minor phase. Two fragments of this sample are present in the thin section and both have breccia matrix attached to basalt.

14304, 187: This sample is a coarse grained basalt displaying an overall ophitic texture containing large euhedral to subhedral plagioclase crystals up to 1mm long (Neal et al., 1989a) (Figure 3c). Olivine is found as both individual grains and as cores in pyroxenes. Interstitial mesostasis glass is present.

14304, 189: This is a granular basalt with a relict subophitic texture (Neal et al., 1989a) (Figure 3d). Large pyroxenes ≥1mm in length and plagioclase 0.5 mm long form an interlocking texture. Two fragments are present in the thin section and interstitial glass is found in the both fragments.

14304, 203: This is a fine-grained basalt with acicular and corroded plagioclase up to 0.5mm in length (Neal et al., 1989a) (Figure 3e). Six fragments are present in the thin section and interstitial glass is found in each fragment.

14304, 221: This coarse-grained sample, originally described by Goodrich et al., (1986) is also represented by 2 additional thin sections (299, 326) (Table 1, Figure 3f). Large subophitic basalt clasts are embedded in attached breccia matrix in all

thin sections. Plagioclase crystals are up to 0.7mm in length and pyroxenes up to 1.2mm in length. Olivine crystals are present within the clasts and as grains within the adhering breccia matrix. A small fine-grained clast separate from the basalt clast is present in the breccia matrix in sample ,221. Interstitial glass is found within the small fine-grained clast and sparingly throughout the larger clasts.

14304, 324: This basalt is similar to 14304,221 with a coarse-grained ophitic basalt embedded in attached breccia matrix (Goodrich et al.,1986) (Figure 3g). Plagioclase crystals are approximately 0.5mm long and pyroxenes up to 1.1mm long. Olivine crystals approximately 0.4mm long are present. Interstitial glass is found within the basalt.

14305, 380: This ophitic, fine grain sized clast with acicular plagioclase laths is embedded in attached breccia matrix (Shervais et al., 1985b) (Figure 4a). Plagioclase crystals are up to 0.5mm long and pyroxenes are up to 1mm long. Resorbed olivine cores to pyroxenes are present. Abundant interstitial glass is present in the basalt.

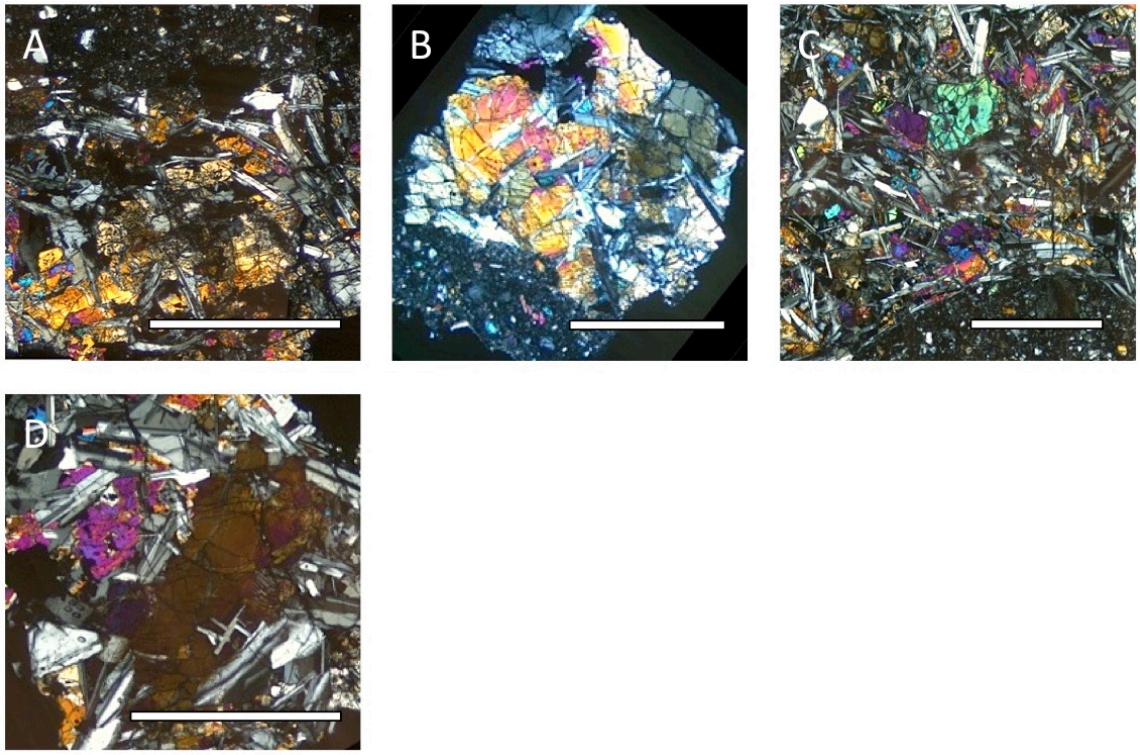

Figure 4. Photomicrographs of VHK basalt clasts from breccia 14305. Scale bar represents 1mm. (a) 14305,380. (b) 14305,383. (c) 14305,388. (d) 14305,393.

14305, 383: This sample is an ophitic fine-grained basalt with adhering breccia matrix (Shervais et al., 1985b) (Figure 4b). Plagioclase laths are up to 0.7mm in length and pyroxenes are ≤0.8mm long A large olivine ~0.7mm in length is surrounded by pyroxene within the clast and small olivine grains are found in the adhering breccia matrix.

14305, 388: This is a coarse grained basalt with an overall subophitic texture (Shervais et al., 1985b) (Figure 4c). Acicular plagioclase laths up to 1mm in length are curved and exhibit a flow texture adjacent to the adhering breccia matrix. Corroded olivine crystals

are present as the cores of pyroxenes and as individual grains. Abundant interstitial glass is found within the basalt.

14305, 393: This coarse grained, subophitic basalt is represented by three individual fragments (Shervais et al., 1985b) (Figure 4d). Large euhedral blocky plagioclase crystals are up to 1 mm in length and pyroxenes up to 1.5mm long. Small (0.1mm) olivine grains and intersitital glass are present in all three fragments.

METHODS

Crystal Size Distributions (CSDs): CSDs are constructed by tracing a select crystal phase in photomosaics of thin sections, which prevents any further destruction of a sample beyond the making of the thin section. The size, roundness, and area of each crystal are compared to the entire area of the sample and a diagram of the natural logarithm of the population density against the crystal size is produced. The natural logarithm of the population density against the crystal size results in a negative correlation, the slope and linearity of which provide information into crystal growth rate and residency time. Curved CSDs can indicate crystal accumulation or textural coarsening, while kinked CSDs can indicate magma mixing (mixing of different crystal cargoes) and different cooling rates of the same phase.

Construction of a CSD begins with acquisition of thin section photomicrographs using a petrographic microscope with a 5x objective. Photomicrographs of each sample in reflected, plain polarized, and cross polarized light are used to create photomosaics of each sample and crystals of the mineral of interest are traced and filled in with a solid color in *Adobe Photoshop* on a tablet PC. The length and area of the crystals are converted into a 8-bit Bitmap (BMP) format and exported into an image processing program that measures the length, width,

and area of each crystal (*ImageJ*, available at http://rsbweb.nih.gov/ ij/) (Higgins and Chandrasekharam, 2007). *CSDSlice* (v.4) Excel© database determines the best habit for the crystals based on the length, width, area, and roundness (Morgan and Jerram, 2006). The habit along with the length of and width were entered into *CSDCorrections* (v1.4.1) producing the CSD graph (Higgins, 2000). Samples 14304,189 and 14304,203 are represented by several fragments (two and six, respectively). Creating a CSD on only one fragment of each sample would not produce a statistically viable CSD, but by combining the areas and crystals for each fragment, a statistically significant CSD can be produced. For acicular plagioclase crystals it has been suggested that a statistically significant CSD would require ≥250 crystals (Morgan and Jerram, 2006). Attached breccia matrix and crystals that were truncated by the matrix (or the edge of the sample) were excluded from the CSD construction.

Electron Probe Microanalysis (EPMA): Major element analyses, backscatter electron (BSE) images and elemental maps were collected on a JEOL JXA-8200 electron microprobe at Washington University in St. Louis. Analyses were collected using a 3 μm beam, accelerating voltage of 15 kV and a probe current of ~25 nA. The beam diameter was broadened to ~5 μm for plagioclase crystals and in order to avoid boiling off Na, which was collected first during data acquisition. Additional major element analyses were collected at the University of Notre Dame on a Cameca SX-50 electron microprobe using an accelerating voltage of 15 kV, probe current of 25 nA, an 6 μm beam diameter for pyroxene and olivine analyses, and an 8 -10 μm beam diameter for feldspar and K-rich area analyses.

Laser Ablation Inductively Coupled Plasma Mass Spectrometry (LA-ICP-MS):

Trace element analyses of plagioclase were conducted using a New Wave UP-213 UV laser ablation system with a ThermoFinnigan Element 2 high-resolution magnetic sector ICP-MS at the University of Notre Dame. A laser frequency of 4 Hz, pulse energy of 0.07mJ/pulse, and a spot size of 30 microns in diameter were used. Calcium measured by EPMA was used as an internal standard for each LA-ICP-MS spot analysis. The NIST 612 glass was used as an external calibration standard. Data were exported in ASCII format for reduction using the *Glitter*© software. The background signal was collected for 20 seconds and the data was acquired for 60 seconds. All laser ablation analyses were collected using time-resolved mode and during data reduction the background and data signals were selected visually to ensure that the best signals were measured and any inclusions were avoided. For plagioclase, detection limits were better than 0.2 ppm for La, Rb, Nb, Eu, Tb, Dy, and better then 0.3 ppm for Ce and Nd. Ba and Sr had detection limits of 2.1 and 6.5 ppm respectively, a function of relatively high background counts for these elements.

In order to calculate the plagioclase equilibrium liquid compositions of the VHK basalts, partition coefficients were calculated using Anorthite compositions of individual spot analysis collected with electron probe microanalysis (EPMA) as Anorthite content is a controlling factor of cation substitution in plagioclase (Blundy and Wood, 1991; Bindeman et al., 1998; Tepley et al., 2010). Individual partition coefficients were then calculated using the method of Hui et al. (2011).

RESULTS

Crystal Size Distributions (CSDs): Plagioclase CSDs were created for 6 VHK basalt samples (14303,245, 14304,187, 14304,189, 14304,203, 14304,221, and 14305,388; Figure 5)(see RobertsSE_Supplemental.xlsx). The downturn in each CSD in Figure 5 gives an indication of the detection limit as the smaller populations become difficult to discern, especially when they reach the thin section thickness (0.03 mm). Two samples display kinked or curved (concave-up) CSD profiles (14303,245 and 14305,388). The remaining profiles are generally linear (within error) after about 0.2-0.4 mm.

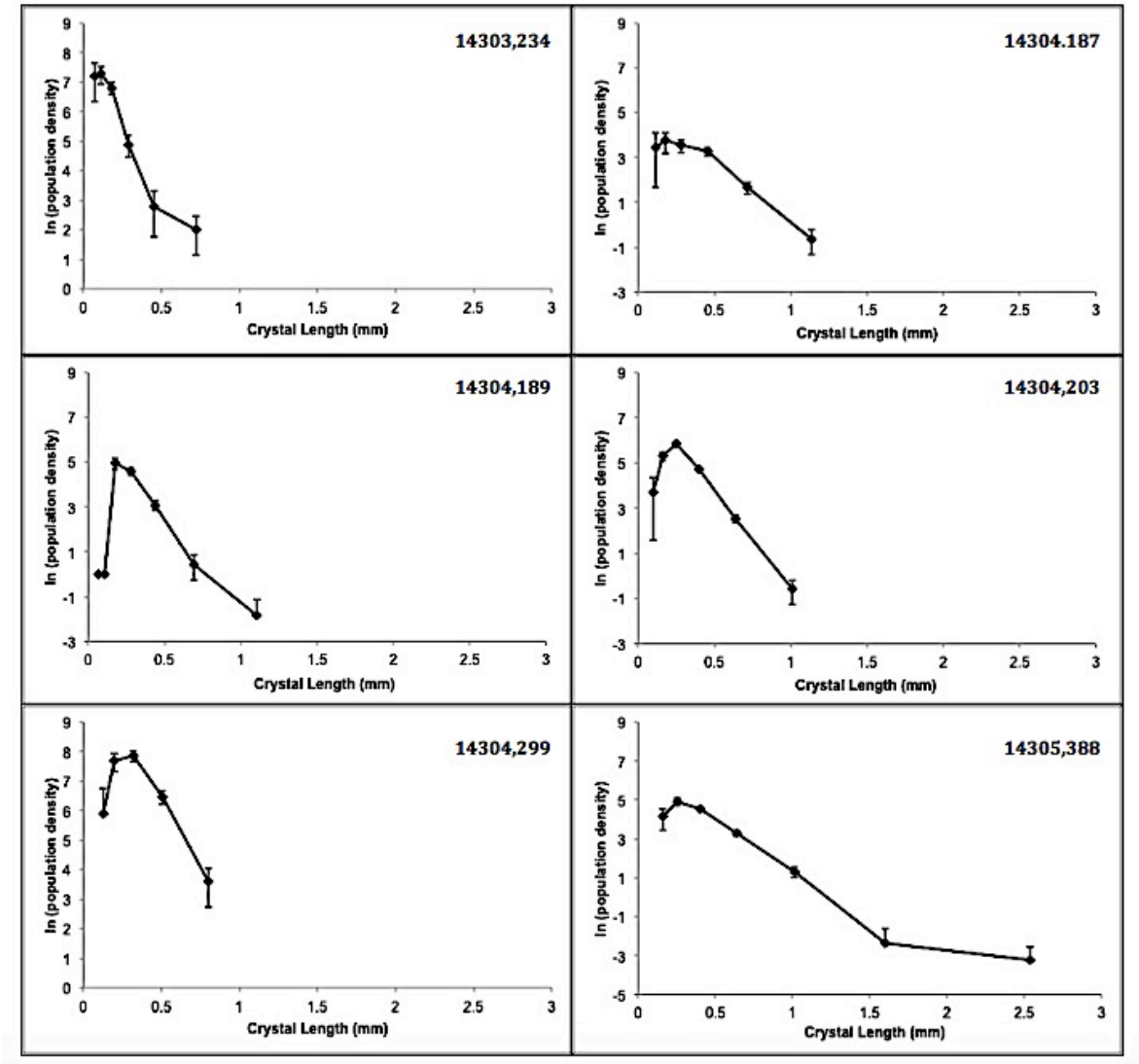

Figure 5. Plagioclase CSDs for six VHK basalts. The CSD for sample 14304,221 is of the small fine-grained clast.

It has been recommended that a minimum of 250 crystals be collected for acicular minerals (Morgan and Jerram, 2006). All but one of the CSDs (14304,203) contain <250 usable plagioclase crystals. Neal et al. (2015) applied two criteria to CSDs that contained less that the recommended number of crystals: (a) a qualitative

evaluation of profile smoothness; and (b) a quantitative evaluation in that errors are ≤10% for at least three consecutive data points. Plagioclase CSDs from 14303,245 and 14304,187 do not meet the first criterion; sample 14304,221 does not meet the second criterion. Therefore, three samples are used in the analysis of plagioclase CSD profiles from VHK basalts: 14304,189, 14304,203, and 14305,388.

Electron Probe Microanalysis (EPMA): Element maps of VHK samples show a heterogeneous distribution of K-rich material among the samples (Figures 6-8). Samples without attached breccia matrix (14304,187, 14304,203, and 14305,393) show K-rich overgrowths on plagioclase while large areas of interstitial glass are less common. Samples with attached breccia matrix show 3 distributions: 1) K-rich areas predominantly within the attached breccia matrix that appear to permeate into the clast in a fluid like manner (14303,328, 14304,221, and 14304,324); 2) large areas of interstitial K-rich material usually associated with plagioclase (14303,245, 14304,169, 14304,177, 14304,187, 14304,189, 14304,203, 14304,383, and 14304,393); and 3) a combination of both K-rich areas within the matrix along with interstitial K-rich areas within the clast (14305,380 and 14305,388).

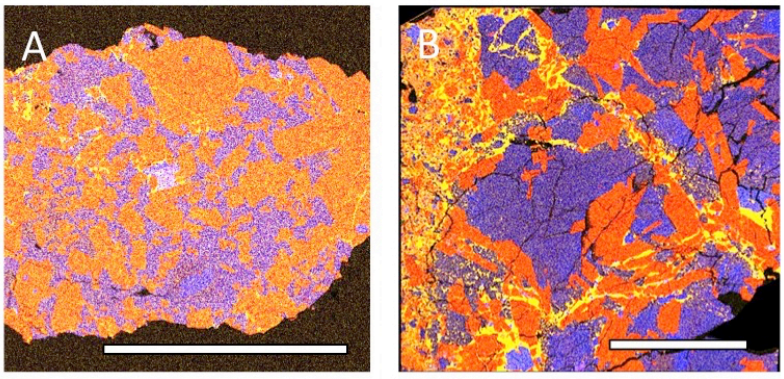

Figure 6. Element maps of VHK basalt clasts from breccia 14303. Red = aluminium, yellow = potassium, and blue = iron. (a) 14303,245. (b) 14303,328. Scale bar represents 1mm.

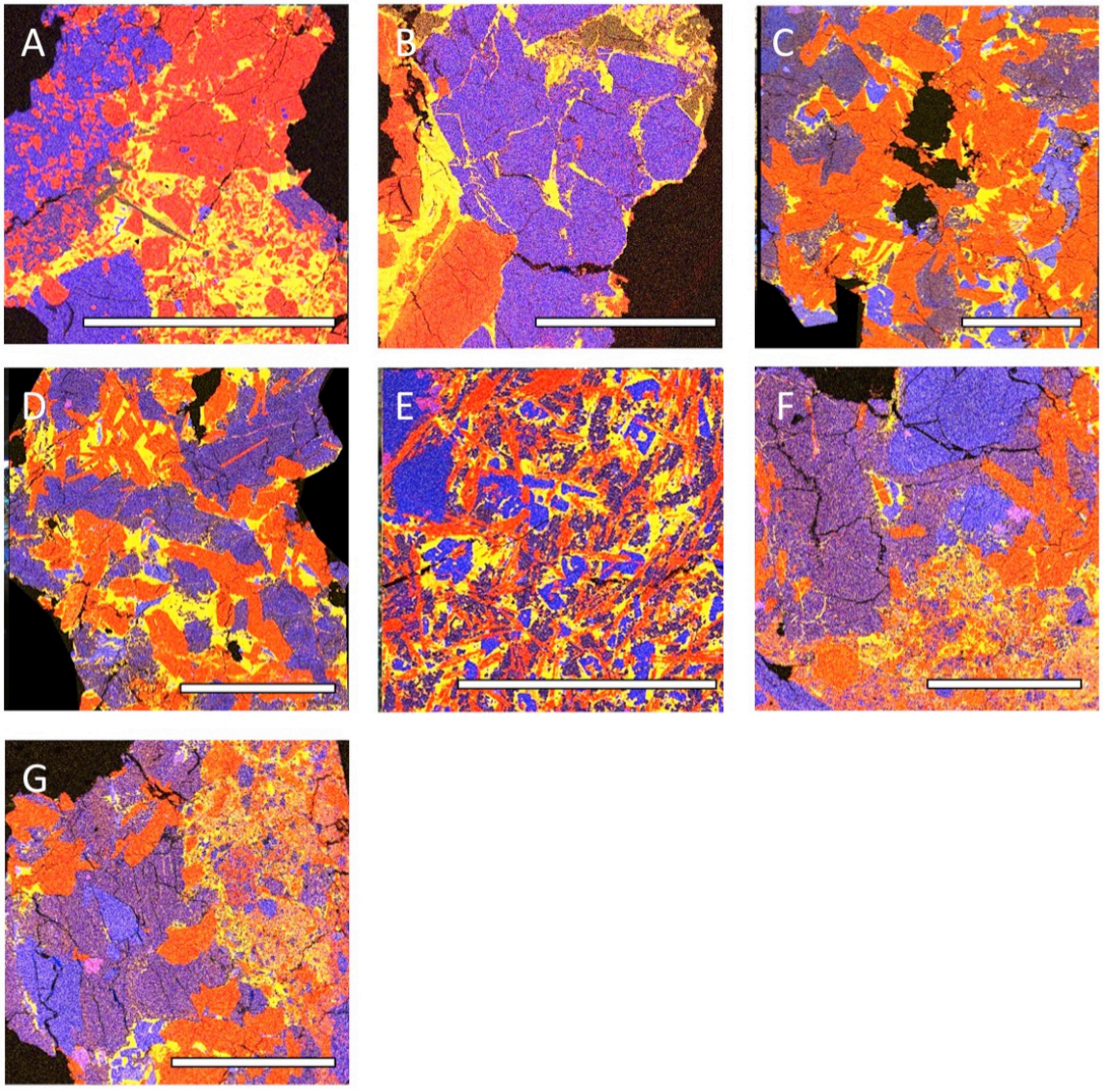

Figure 7. Element maps of VHK basalt clasts from breccia 14303. Red = aluminium, yellow = potassium, and blue = iron. (a) 14304,169. (b) 14304,177. (c) 14304,187. (d) 14304,189. (e) 14304,203. (f) 14304,221. (g) 14304,324. Scale bar represents 1mm.

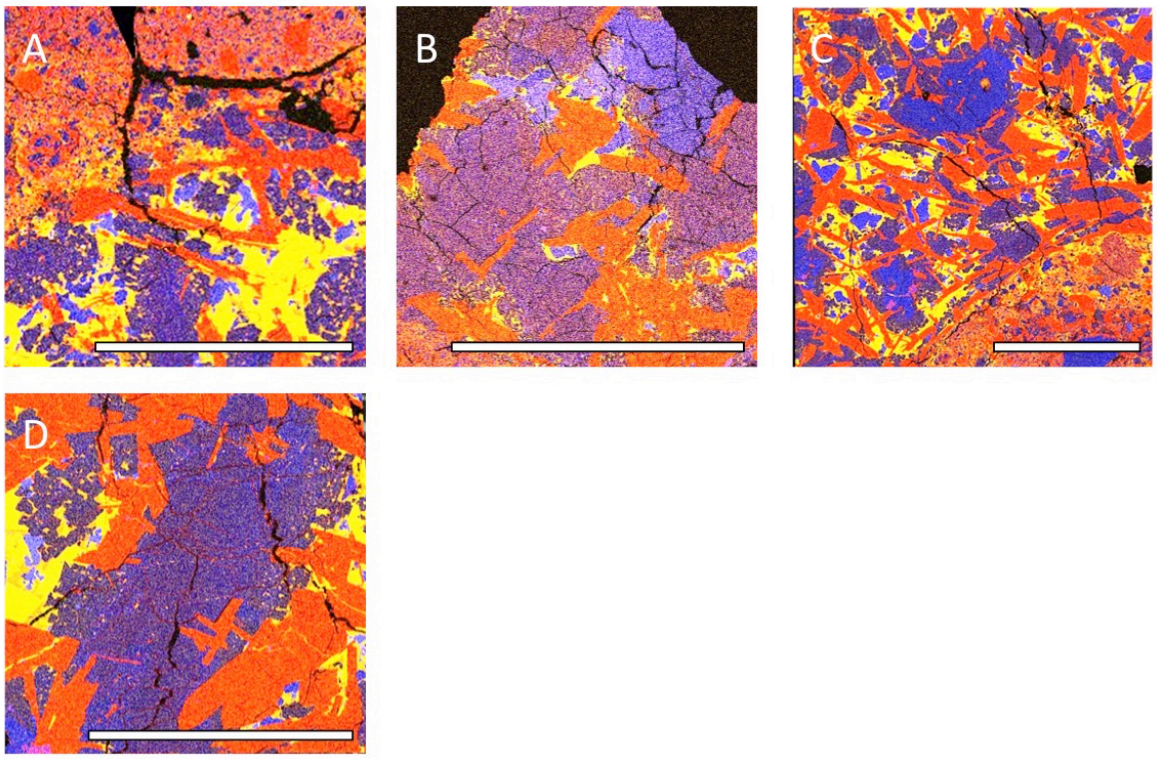

Figure 8. Element maps of VHK basalt clasts from breccia 14303. Red = aluminium, yellow = potassium, and blue = iron. Scale bar represents 1mm. (a) 14305,380. (b) 14305,383. (c) 14305,388. (d)14305,393.

Plagioclase compositions range from An_{61} to An_{97}, with an average of An_{93} (see RobertsSE_Supplemental.xlsx). The most An-poor compositions occur towards the rims of the larger plagioclase crystals and in the smaller groundmass crystals. Olivine compositions range Fo_{21} to Fo_{68} with an average of Fo_{42}. There does not appear to be a bimodal distribution of olivine compositions (Fo-rich and Fa-rich populations) as reported by Shervais et al. (1985b) with a continuum being apparent. Pyroxene compositions range from enstatite and pigeonite (En26-66; Wo1-19) to augite (Wo20-42; Fs21-39). Analyses of K-rich areas as identified by the

element maps range from 6 to 15 wt % K_2O with an average of 12 wt % K_2O. BaO concentrations range from 0 to 5.4 wt %. The weight percentages of oxides measured in the K-rich areas were normalized to 8 oxygens in an attempt to differentiate crystalline K-feldspar from K-rich glass using the structural formula of feldspar. Spot analyses on K-rich areas with cation values of <4.9 (and elevated FeO and MgO above 0.5 wt%) are assigned the designation of glass. BaO abundances of >1 wt % are found in K-rich areas with approximately > 13 wt % K_2O.

Laser Ablation Inductively Coupled Plasma Mass Spectrometry (LA-ICP-MS): Trace element analyses of plagioclase crystals from VHK basalt 14303,245 were collected via LA-ICP-MS in the Midwest Isotope and Trace Element Research Analytical Center (MITERAC) at Notre Dame (see RobertsSE_Supplemental.xlsx). Plagioclase compositions between of the different LA-ICP-MS analyses show little major element variation (An_{91-95}). Spots 245-2 and 245-3 both show elevated concentrations of Nb, Rb, Eu, Gd, Tb, Dy, Yb, and Lu, and the analyses were taken in the center of the plagioclase, however other measurements taken at the center of crystals do not reflect this trend and no correlation is present with anorthite content. Elevated trace element concentrations and a 'flat' trace element profile shown in analysis 245-13 suggest that a mineral inclusion within the plagioclase crystal was encountered during the analysis. These counts were omitted from the final data integration.

DISCUSSION

Crystal Size Distributions (CSDs): The CSDs shown in Figure 5 can be compared to other lunar basaltic samples following the method of Neal et al. (2015). The linear portion of the CSD ≥0.3 mm with a constant gradient is used (where the errors are <15%) to compare plagioclase CSDs from different samples. After the data has been refined, the slope and the y-axis intercept are determined and these are plotted against each other. This method discriminates impact melts from endogenous mare basalts and is applied to the VHK basalts (Figure 9).

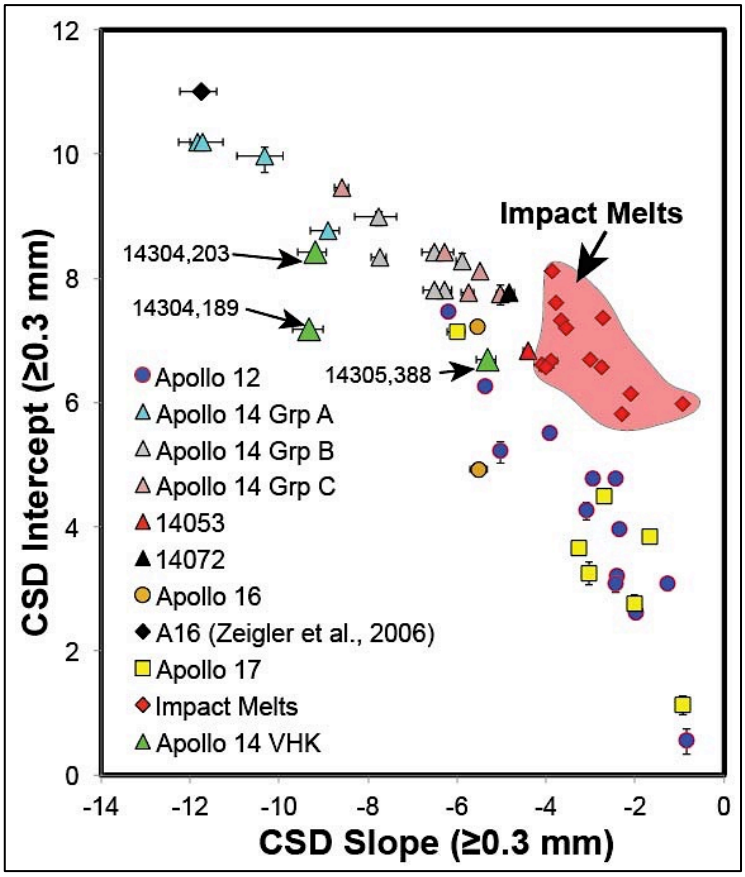

Figure 9. Plagioclase CSD slope vs intercept graph.

The plagioclase CSDs for samples 14305,388 and 14304,203 have steep slopes and relatively high y-axis intercepts, similar to, but slightly below, the Apollo 14 high-Al basalts on a plot of plagioclase CSD slope vs. CSD intercept plotted following the criteria outlined in Neal et al. (2015) (Figure 9). Sample 14304,189 falls below the Apollo 14 high-Al basalts in Figure 9, but does not plot within the impact melt field. The conclusion is that the Apollo 14 VHK basalts, at least represented by the three basalts plotted in Figure 9, are pristine endogenous lunar basalts that are similar to the Apollo 14 high-Al basalts.

Electron Probe Microanalysis (EPMA): A detailed petrographic study of Apollo 14 VHK basalts, using both conventional petrographic and elemental mapping techniques, have produced results that suggest an alternative method of K enrichment to granite assimilation in at least some VHK basalts (Roberts and Neal, 2014a,b, 2015). K-rich veins penetrate broken plagioclase grains in sample 14303,328 (Figure 5) yet the pyroxene grains are intact and absent of K-rich veins. This observation is consistent with feldspar grains experiencing shock metamorphism in impact events while pyroxenes are unaffected (Jaret et al., 2015). Some samples have large amounts of K within the attached breccia matrix and fluid-like veins penetrating the VHK basalt samples (e.g., 14303,328; Figure 5). Although the K-rich areas in the breccia matrix are inherently small and difficult to analyze, three analyses were possible and show that the matrix K-rich areas are compositionally indistinguishable from those within the basalt clast. Observations such as these suggest that K enrichment could be a secondary process unrelated to basalt petrogenesis. Here, we hypothesize that at least in some VHK samples the enrichment of K in otherwise high-Al basalts was impact generated and that the K enrichment of some of the basalts described as "VHK" occurred during breccia formation, with the K-rich material being derived from the breccia matrix. Given the textural relationship of the K-rich glass to the basaltic crystal phases and the breccia matrix suggests it infiltrated the basalt after inclusion of the clasts in the breccia. We hypothesize that after breccia formation it was covered in a hot impact melt sheet that melted the low melting point components, such as K-feldspar with a melting point of 1215 K, well below the heat generated by an impact ~1500˚C (Larson 1929;

Stoffler 1984). K-feldspar is also present in Apollo 14 breccias (e.g., Warren et al., 1983). The K-rich impact melt infiltrated high-Al basalt clasts, preserving the basaltic texture, but altering the whole-rock chemistry. A similar hypothesis was suggested by Goodrich et al. (1986) after observing K-rich vein areas in an alkali norite clast from breccia 14304. This melt that moved through breccia 14304 would not discriminate between clasts and could contaminate any original composition. This hypothesis is supported by the plagioclase CSDs that indicate a formation through endogenous igneous processes (Figure 9).

Not all previously classified VHK basalt clasts exhibit a textural relationship that would suggest secondary K enrichment through a pervading, impact-induced melt, indicating that VHK basalt generation through endogenous igneous processes (i.e., granite assimilation) is still a viable process for generating at least some of the VHK basalts. Granite is available for assimilation as it has been returned from all Apollo missions with the exception of Apollo 11 and 16 (e.g. Blanchard et al., 1977; Martinez 1989; Quick et al., 1977; Seddio et al., 2013) and is present at the Apollo 14 site (Warren et al., 1983). It is apparent from the element map for sample 14305,388 (Figure 8c) that the K-rich material in the basalt is distinct from that in the breccia matrix. Therefore, textural evidence suggests the VHK basalts be divided into two groups on the basis of the relationship of K-rich phases in the basalt and breccia matrix.

Major element analyses of K-rich areas indicate two modes of K enrichment within the VHK basalts: interstitial mesostasis glass and K-feldspar (Figure 10). VHK basalts clasts that contain fluid-like K-rich veins also have elevated BaO, suggesting

that the source of the BaO was externally derived and secondary to the petrogenesis of the basalt. Alternatively, the VHK basalt clasts could be the source of the K-rich areas in the breccia matrix. Partial melting of K-feldspar within the VHK basalts would produce K-rich glass with low Ba contents (Figure 10) as Ba is strongly partitioned into residualK-feldspar (e.g., Fedele et al., 2015). The textures are interpreted such that some samples obtained K (and Ba) enrichment through AFC with granite and others obtained the VHK signature after remobilization of K-rich material that occurred during breccia formation.

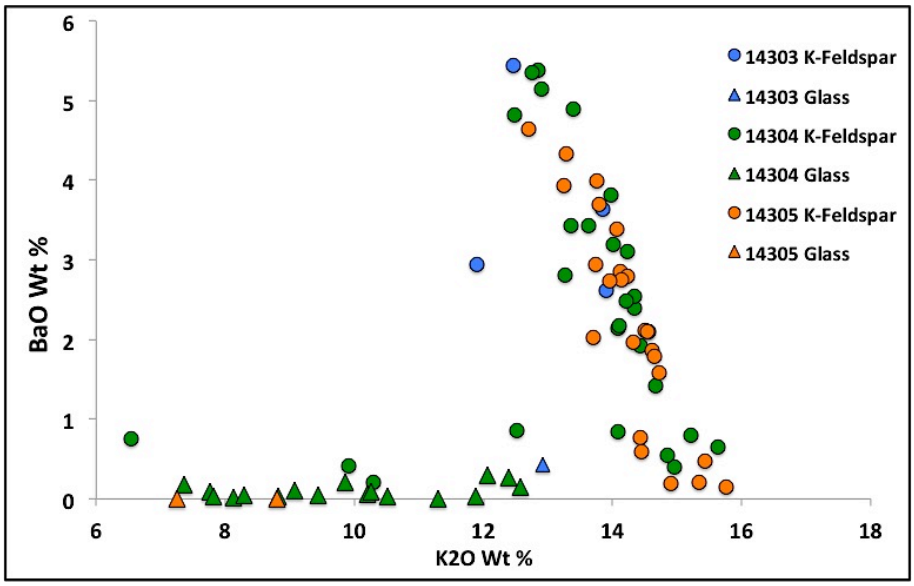

Figure 10: K-rich phase compositions from breccias 14303, 14304, and 14305

Laser Ablation Inductively Coupled Plasma Mass Spectrometry (LA-ICP-MS): In-situ trace element analysis of plagioclase crystals from VHK basalt 14303,245, were collected via LA-ICP-MS in effort to demonstrate the relationship between high-Al basalts and VHK basalts regardless of secondary granite infiltration (Roberts and Neal, 2014b). Chemical evolution of a magma can be recorded in plagioclase while it is on the liquidus (Bindeman and Bailey, 1999). Only olivine precedes plagioclase as a liquidus phase, but it does not fractionate rare earth elements or incompatible trace elements, therefore, plagioclase is capable of preserving the original ratios of parental magma incompatible trace elements. Partition coefficients were calculated using anorthite compositions of individual spot analysis collected with electron probe microanalysis (EPMA) (*cf*. Hui et al., 2011). When compared to high-Al basalt plagioclase data from Hui et al. (2011), equilibrium liquids calculated for the plagioclase crystals of VHK basalt 14303,245, were similarly enriched in Sr and La/Ce as equilibrium liquids of plagioclase from Apollo 14 high-Al Group B and C basalts (Figure 11). In situ analyses are the key to seeing past the secondary impact-derived granite contamination and determining the petrogenetic relationship between high-Al and VHK basalts.

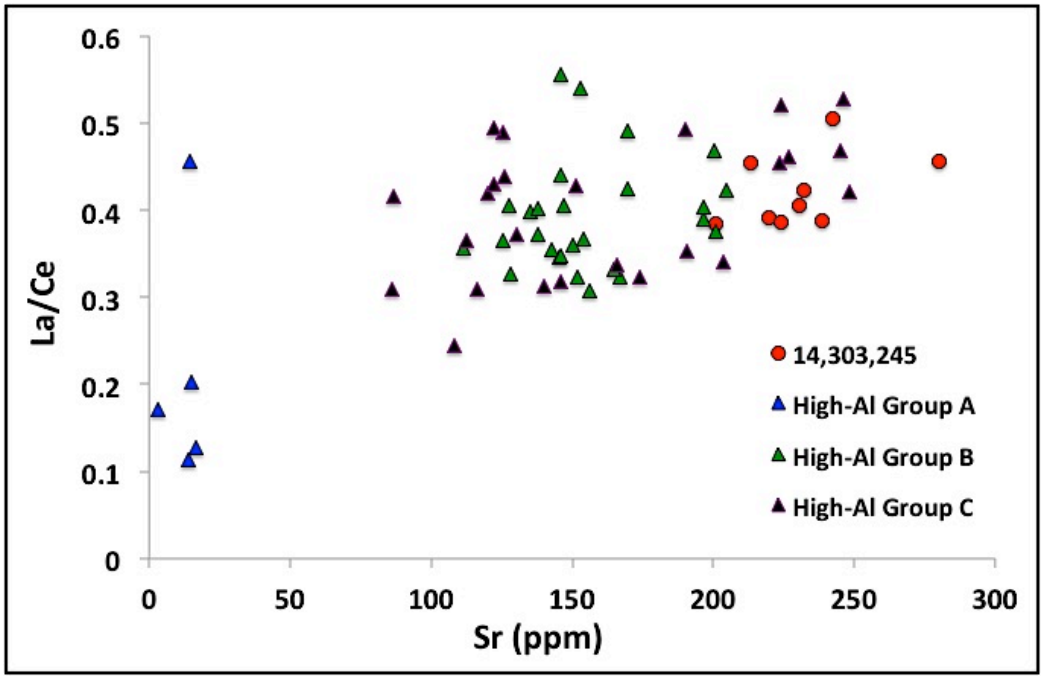

Figure 11: Calculated Sr and La/Ce concentrations of melts equilibrated in plagioclase crystals in VHK sample 14303,245 compared to plagioclase equilibrium liquids from Apollo 14 high-Al Group A, Group B, and Group C basalts. Plagioclase data from high-Al basalts are taken from Hui et al. (2011).

The assimilation of granite by high-Al basalts can be tested by examining the physical properties of the magmas as such a petrogenesis should produce basalts that have a decreased density and an increased viscosity relative to high-Al basalts. To test this hypothesis, the viscosities of the VHK basalts were calculated using whole rock compositions following the method of Giardano et al. (2008) and the densities were calculated using the method of Bottinga and Weill (1970). Also included in these calculations were K-feldspars from various lunar lithologies, to test the hypothesis that selected remobilization of K-feldspar (low melting point material) could account for the textures where the K-rich material appears to be permeating onto the clast from the breccia matrix. When compared to the calculated viscosities and densities of Apollo 14 high-Al basalts, lunar granites, and K-feldspar, VHK basalts fall into two groups: those that have viscosities and densities similar to the Apollo 14 high-Al basalts (VHK-1 in Figure 12), and those that have higher viscosities and lower densities than the high-Al basalts (VHK-2 in Figure 12) (Table 2.). It is difficult to reconcile the VHK-1 samples with the granite assimilation model, whereas the compositions forming the VHK-2 grouping are consistent with the granite AFC model.

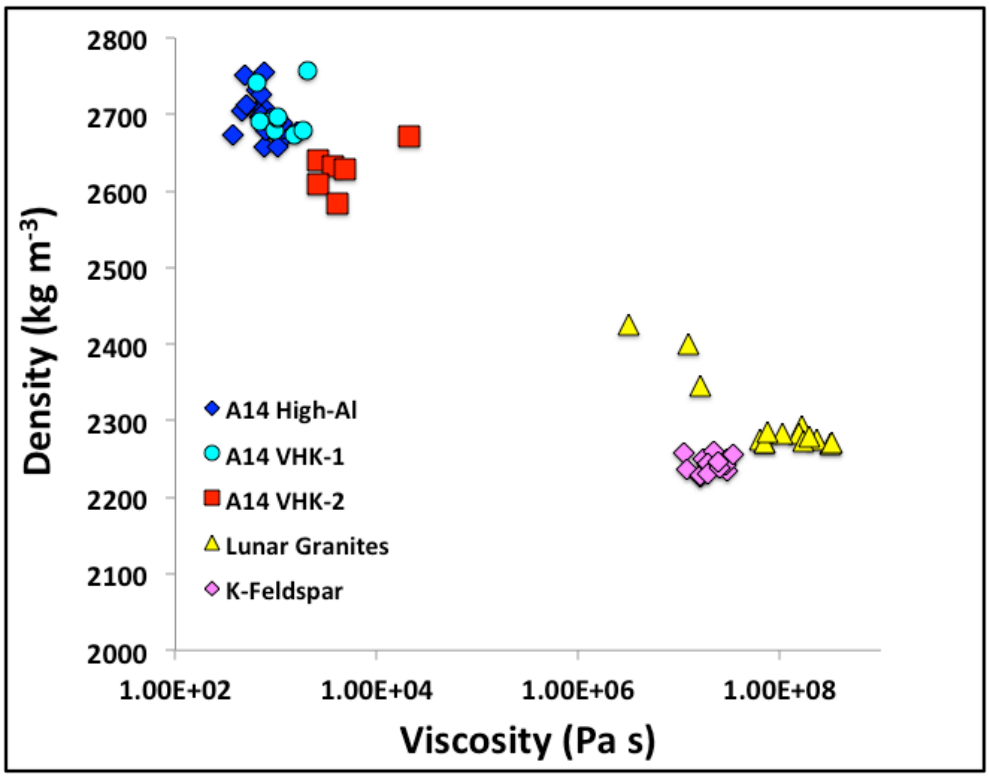

Figure 12. Density and viscosity of VHK basalts compared to Apollo 14 high-Al basalts, Lunar granites, and K-Feldspar. Data are from Warren et al. (1983, 1986, 1997); Warner et al. (1980); Neal (2001); Neal et al. (1988, 1989b); Shervais et al. (1983, 1985a,b); Ma et al. (1980); Compston et al. (1972); Seddio et al. (2013); Jolliff et al. (1999); Peckett (1972); Neal and Kramer (2006); Lin et al. (2012).

TABLE 2

VHK-1 AND VHK-2 BASALT SAMPLES AS DESIGNATED BY DENSITY AND VISCOSITY

VHK-1		
Breccia	Whole-Rock Sample No.	Probe Mount No
14168	38	39
14181	6	
14303	318	328
14304	148	187
14304	180	203
14305	370	343,344
14305	380	373
14305	390	393
14305	384	383
VHK-2		
14303	247	246
14304	152	189
14304	164	194
14304	168	169
14304	176	177
14305	382	388

It is evident that the VHK basalts comprising the VHK-1 group in Figure 12 show great similarities with the Apollo 14 high-Al basalts. Creating the "VHK" signature of the VHK-1 basalts through granite assimilation is difficult. It is also evident that while all VHK basalts show an enrichment of K_2O over the Apollo 14 high-Al basalts (Figure 13a), all but two of the samples comprising the VHK-1 group have Ba contents similar to the high-Al basalts (Figure 13b). As can be seen from Figure 12, VHK-1 basalts cannot be generated through assimilation of bulk lunar granite or selective assimilation of K-feldspar. A new model is presented to explain these new observations.

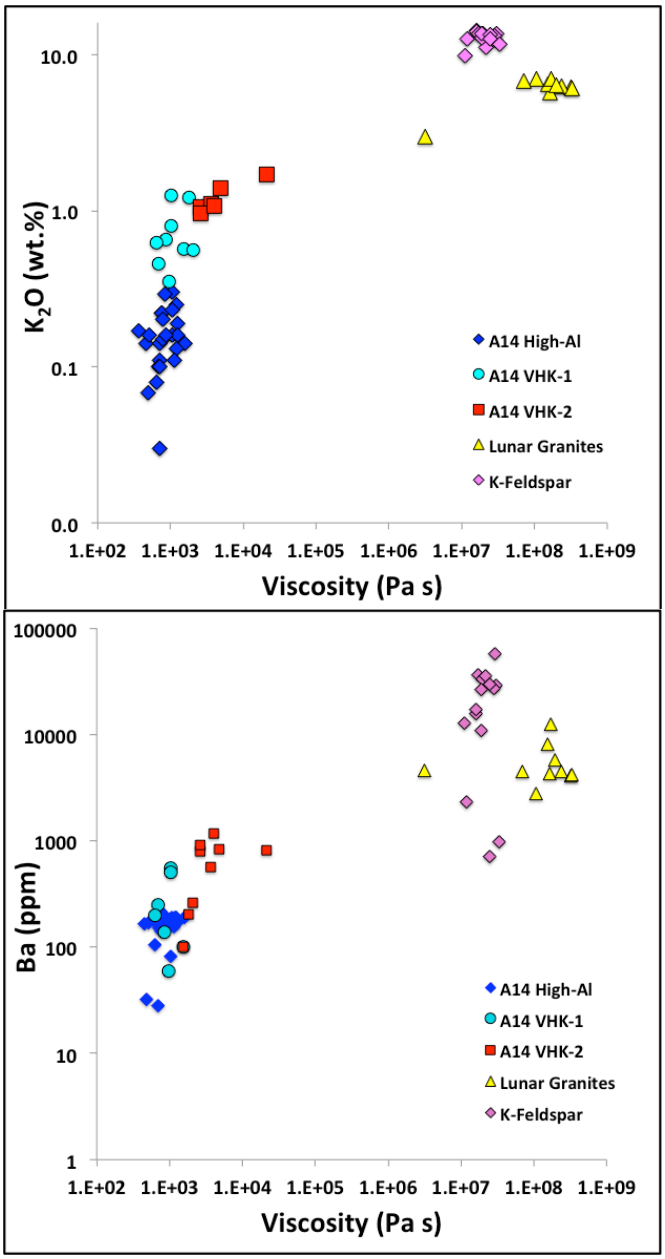

Figure 13. Plots of viscosity vs. K_2O (top) and Ba (bottom) for the Apollo 14 VHK basalts compared to the Apollo 14 high-Al basalts, lunar granite and lunar K-feldspar compositions. The two VHK basalt groups are defined on the basis of viscosity and density considerations in Figure 11. Data are from Warren et al. (1983, 1986, 1997); Warner et al. (1980); Neal (2001); Neal et al. (1988, 1989b); Shervais et al. (1983, 1985a,b); Ma et al. (1980); Compston et al. (1972); Seddio et al. (2013); Jolliff et al. (1999); Peckett (1972); Neal and Kramer (2006); Lin et al. (2012).

It is evident from Figure 13 that the high Ba contents of lunar granites are contained in the K-feldspar and Celsian components. However, simple mixing of K-feldspar and a high-Al basalt composition cannot produce the VHK-1 basalt compositions. To account for the VHK-1 basalt observations from this study, enrichment through vapor deposition is posited. Formation of breccias 14303, 14304, and 14305 requires impacts to create the various clast populations and subsequent impacts to weld the breccia. It is during the welding process in a hot impact-generated regolith blanket that the fractionation of K from Ba can occur and the high-Al basalts become enriched in K without affecting the physical properties (i.e., viscosity and density). K-feldspar begins to melt around 1100˚C, although this temperature is lower if it is present in a granite. Ahrens and O'Keefe (1972) noted that under shock melting, K-feldspar melts at a lower temperature than quartz. It is during the dissociation of K-feldspar that K can be boiled off. Examining the boiling points of K and Ba, they are ~760˚C and (Haynes, 2011) and 1640˚C (Zhang et al., 2011), respectively. This produces the relationships of VHK-1 basalts observed in Figures 13 and 14. VHK-2 basalts are produced by assimilation of granite by a high-Al parent magma.

If selective K fractionation from Ba is possible through impact generated heat and vaporization, then K fractionation from elements similar to Ba should exhibit the same behavior. K/Sr ratios should be similar to those of K/Ba ratios for VHK-1 and VHK-2 basalts, however the lack of Sr whole rock data and the large detection limits for the Sr data that are available (through instrumental neutron activation) do not allow for this comparison. Instead, K/La ratios are used to illustrate in Figure

15 the selective enrichment of K from La in VHK-1 basalts.

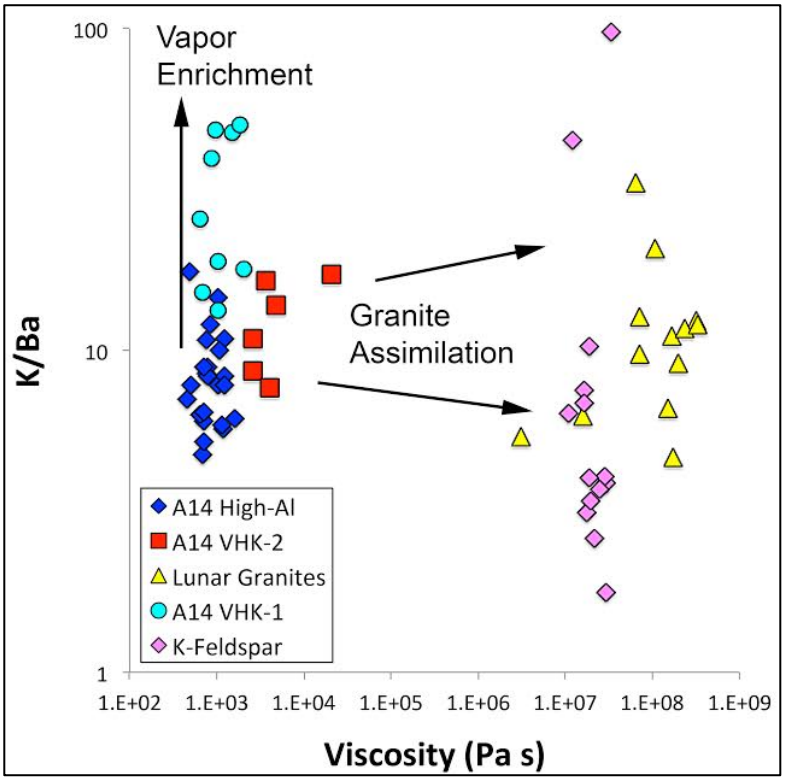

Figure 14. K/Ba and viscosity of VHK basalts compared to Apollo 14 high-Al basalts, Lunar granites, and K-Feldspar. Data are from Warren et al. (1983, 1986, 1997); Warner et al. (1980); Neal (2001); Neal et al. (1988, 1989b); Shervais et al. (1983, 1985a,b); Ma et al. (1980); Compston et al. (1972); Seddio et al. (2013); Jolliff et al. (1999); Peckett (1972); Neal and Kramer (2006); Lin et al. (2012).

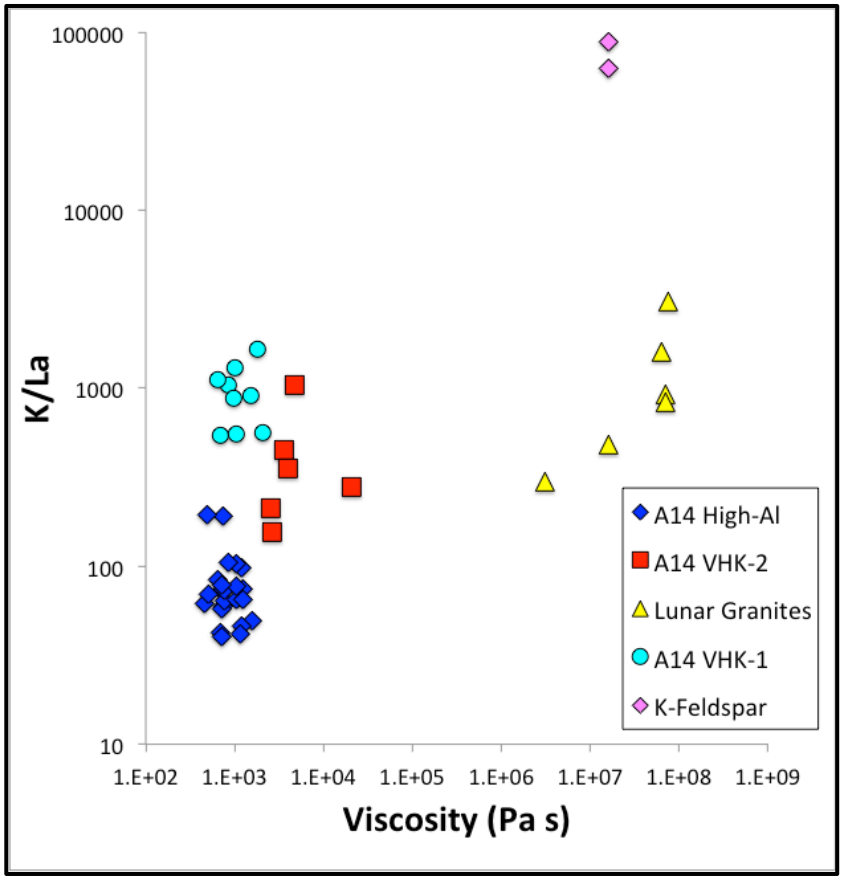

Figure 15. K/La and viscosity of VHK basalts compared to Apollo 14 high-Al basalts, Lunar granites, and K-Feldspar. Data are from Warren et al. (1983, 1986, 1997); Warner et al. (1980); Neal (2001); Neal et al. (1988, 1989b); Shervais et al. (1983, 1985a,b); Ma et al. (1980); Compston et al. (1972); Seddio et al. (2013); Jolliff et al. (1999); Peckett (1972); Neal and Kramer (2006); Lin et al. (2012).

One sample, 14303,245, is not a VHK basalt as originally classified (Neal et al., 1988). The relatively high K_2O for this sample was reported as "<0.75 wt.%" from instrumental neutron activation data (Neal et al., 1988), which was interpreted to be an upper limit not an absolute value due to counting statistics after sample irradiation. Therefore, this sample could contain a K_2O abundance that negates its

classification as a VHK basalt, or there was K-rich breccia matrix adhering to the aliquot analyzed for the whole rock composition. The lack of K-rich mesostasis material in the elemental map for this sample (Figure 6a) is consistent with this sample being removed from the VHK basalt classification.

CONCLUSION

The identification of two groups of VHK basalts that are produced by two different methods of K enrichment resolves the previous difficulties found in modeling the petrogenesis of VHK basalts. A relationship between Apollo 14 high-Al and VHK basalts has been apparent from the detailed petrographic and mineralogic study presented here. It is evident that petrogenetic models developed using whole-rock data have not shown the full petrogenetic history of VHK basalts. Granite obviously plays an important role in VHK basalt petrogenesis whether it is from the assimilation into a high-Al basalt magma to create a purely endogenous VHK basalt or a secondary impact-induced enrichment process to create an impact-enriched VHK basalt (Shervais et al., 1985b; Shih et al., 1986; Neal et al., 1988, 1989; Roberts and Neal, 2014b). These two entirely different modes of formation produce basalts with similar whole rock compositions. Only by investigating the physical properties of these samples can the distinction be made.

The relationship of the clasts through the breccias they were found in has lead to the previous assumption of relationships within lava flows. This imposed relationship needs to be reconsidered in light of new results. Similar trends of K-rich material in other non-VHK basalt clasts, such as the alkali norite described by

Goodrich et al. (1986), needs to be discovered to comment on the mobility and distribution of K-rich (and potential other) material throughout lunar breccias.

APPENDIX A

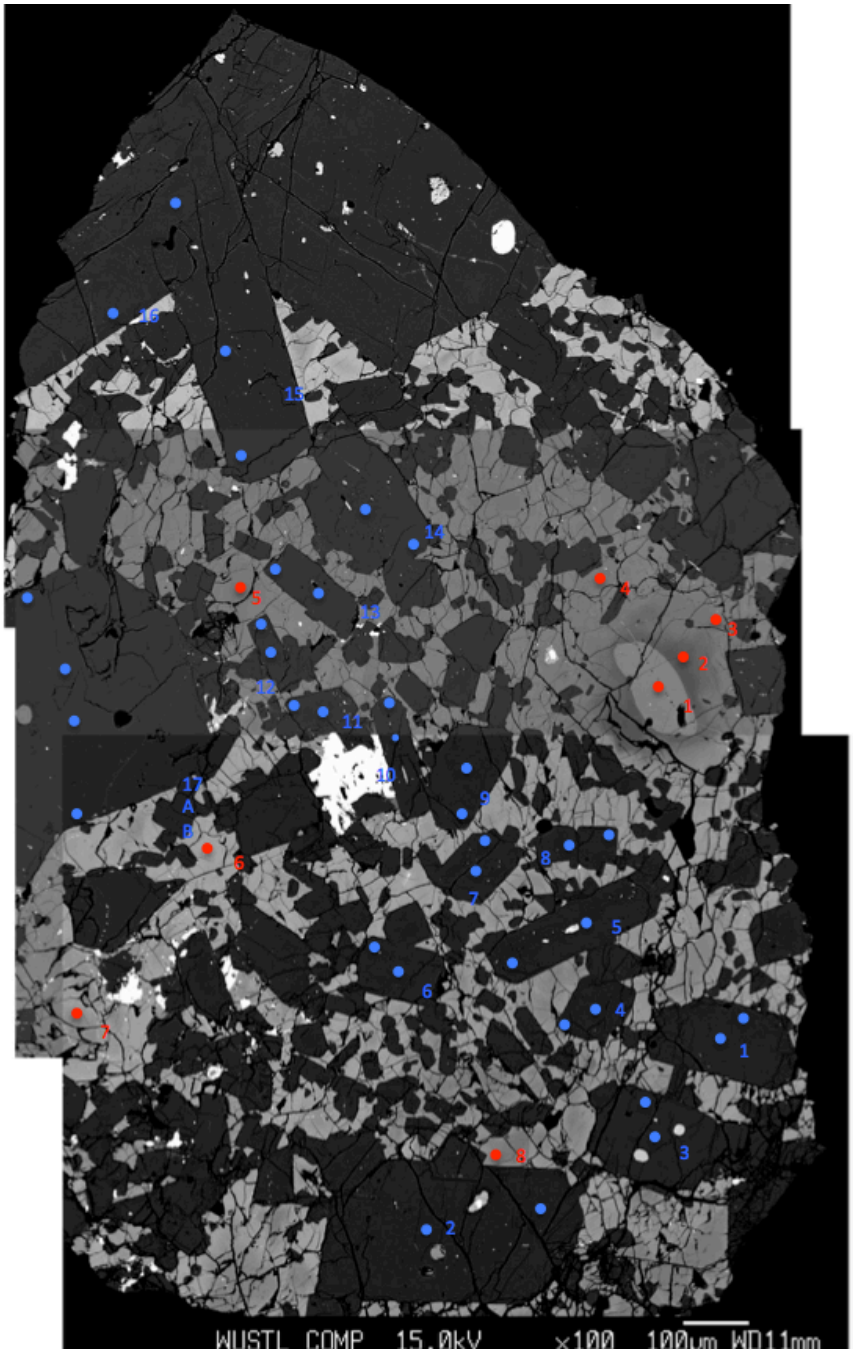

Figure A.1: EPMA map for 14303,245. Blue dots = plagioclase and red dots = pyroxenes.

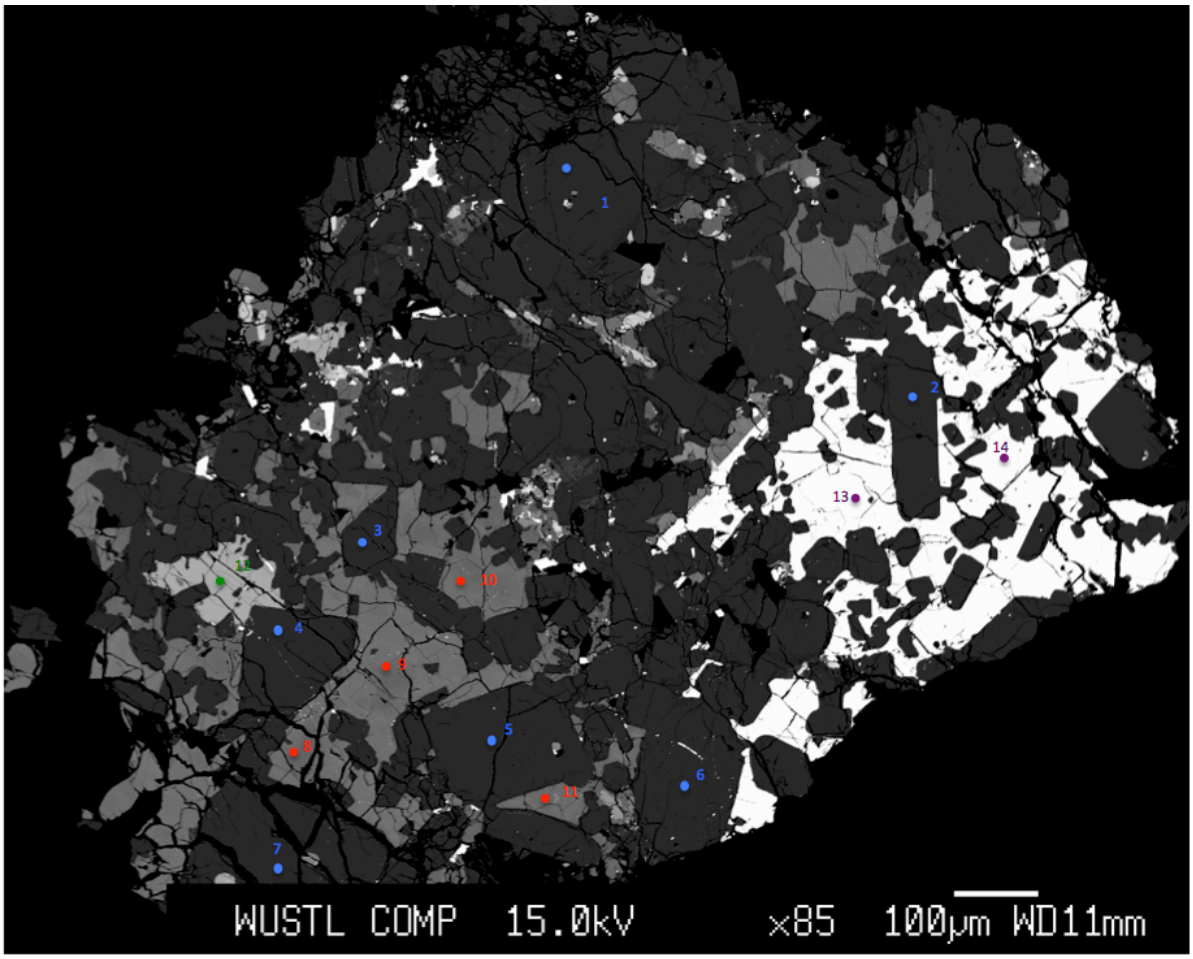

Figure A.2: EPMA map for 14303,245b. Blue dots = plagioclase and red dots = pyroxenes,

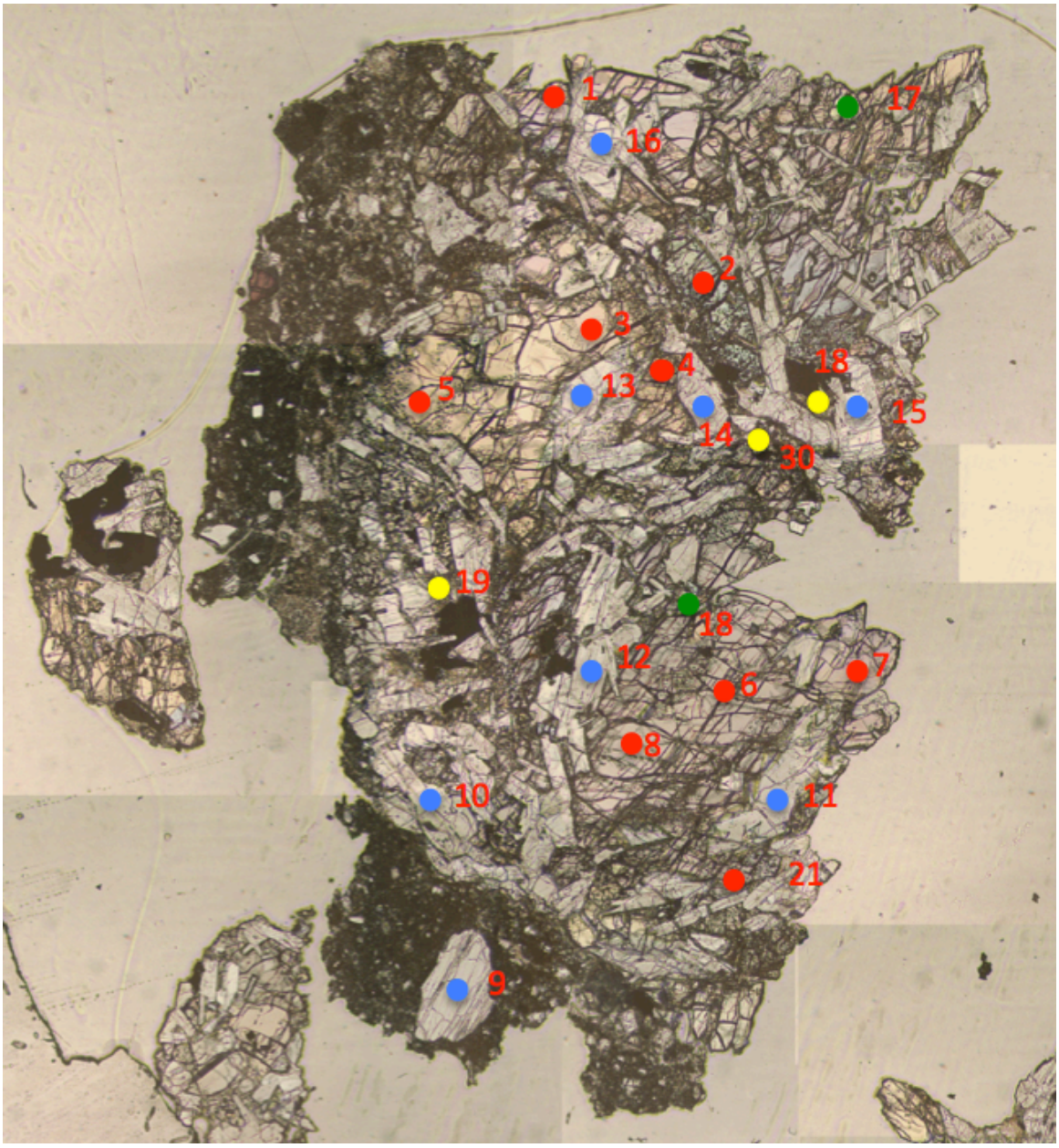

Figure A.3: EPMA map for 14303,328. Blue dots = plagioclase, red dots = pyroxenes, green dots = olivine, and yellow dots = K-feldspar.

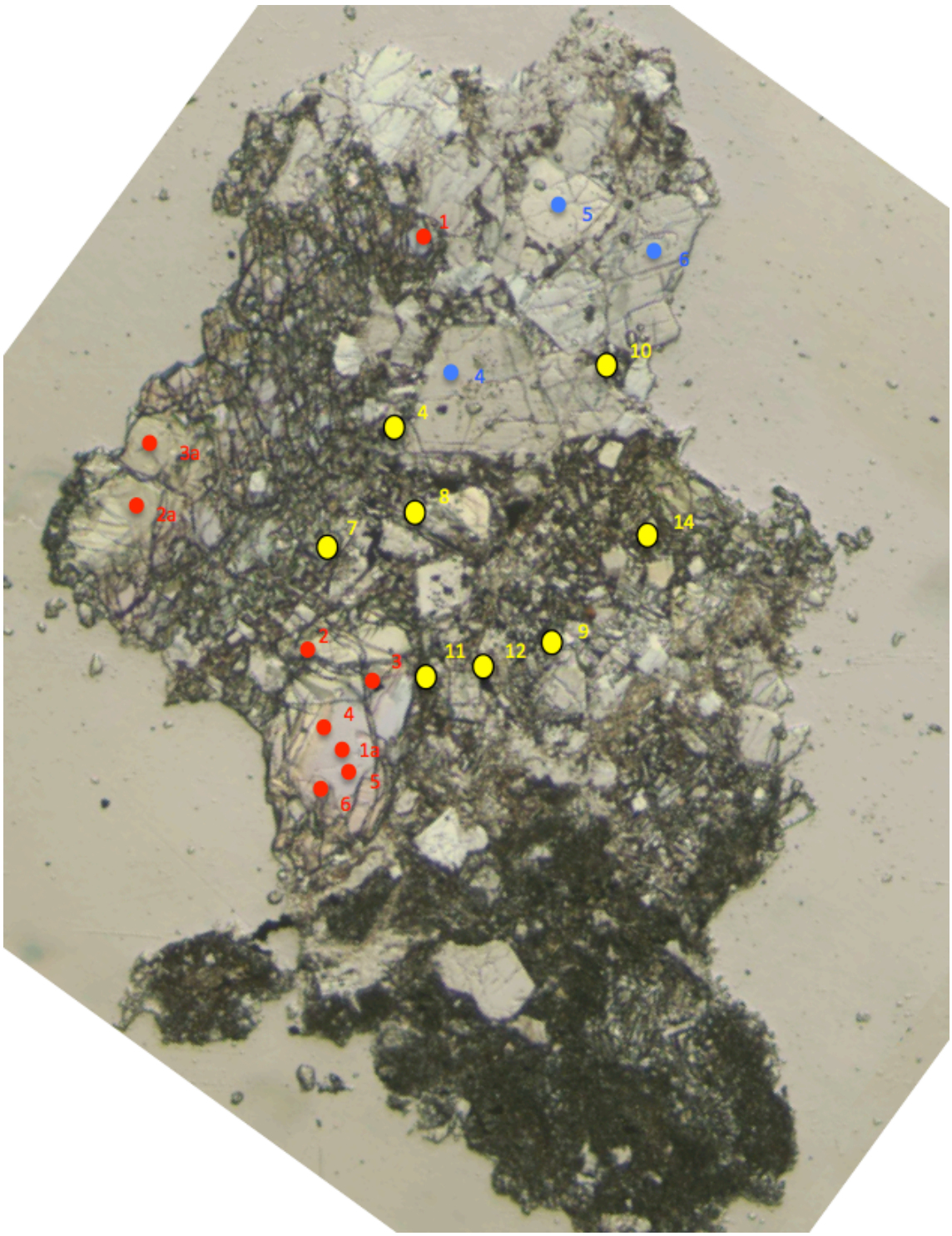

Figure A.4: EPMA map for 14304,169_1. Blue dots = plagioclase, red dots = pyroxenes, and yellow dots = K-Feldspar.

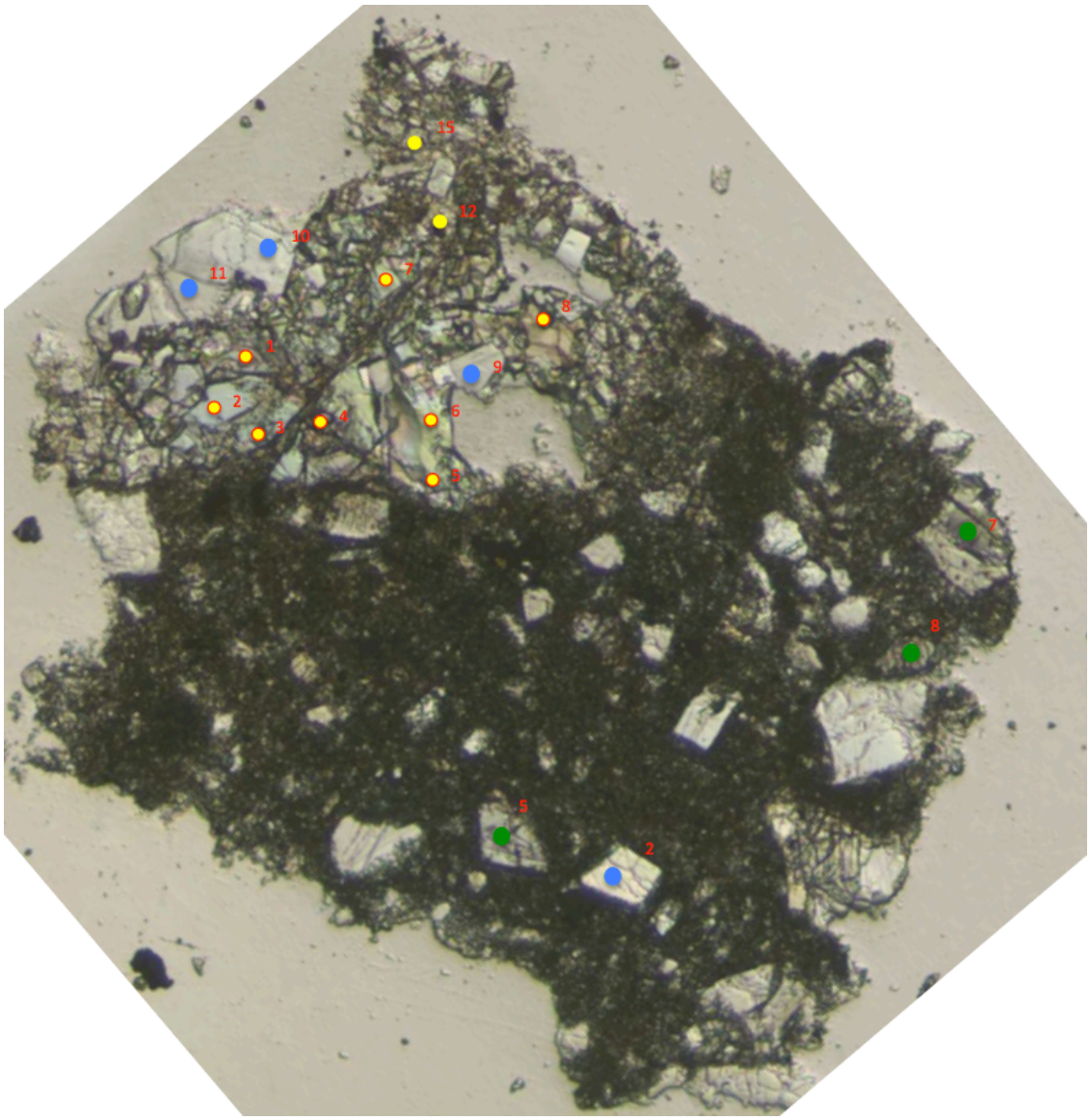

Figure A.5: EPMA map for 14304,169_2. Blue dots = plagioclase, red rimmed dots = pyroxenes, green dots = olivine, and yellow dots = K-Feldspar.

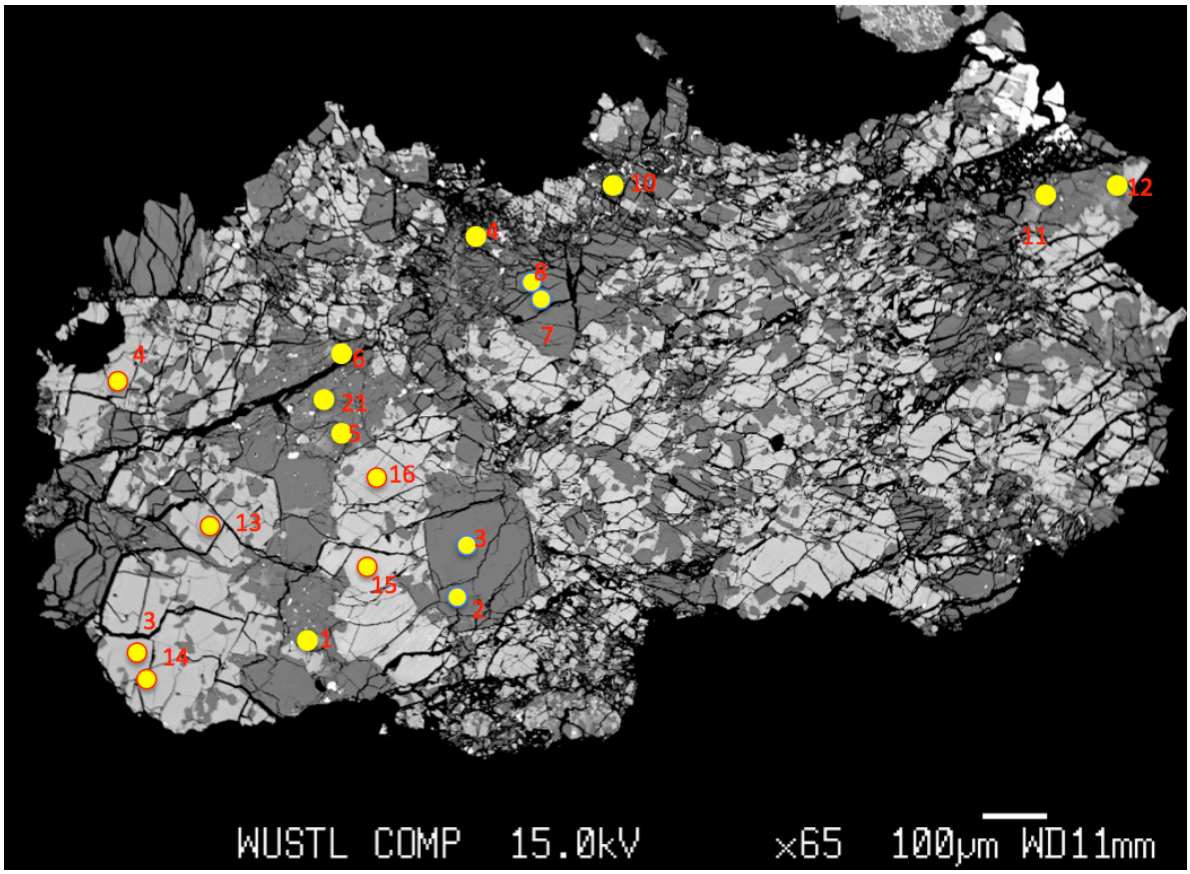

Figure A.6: EPMA map for 14304,269_3. Blue rimmed dots = plagioclase, red rimmed dots = pyroxenes, and yellow dots = K-Feldspar.

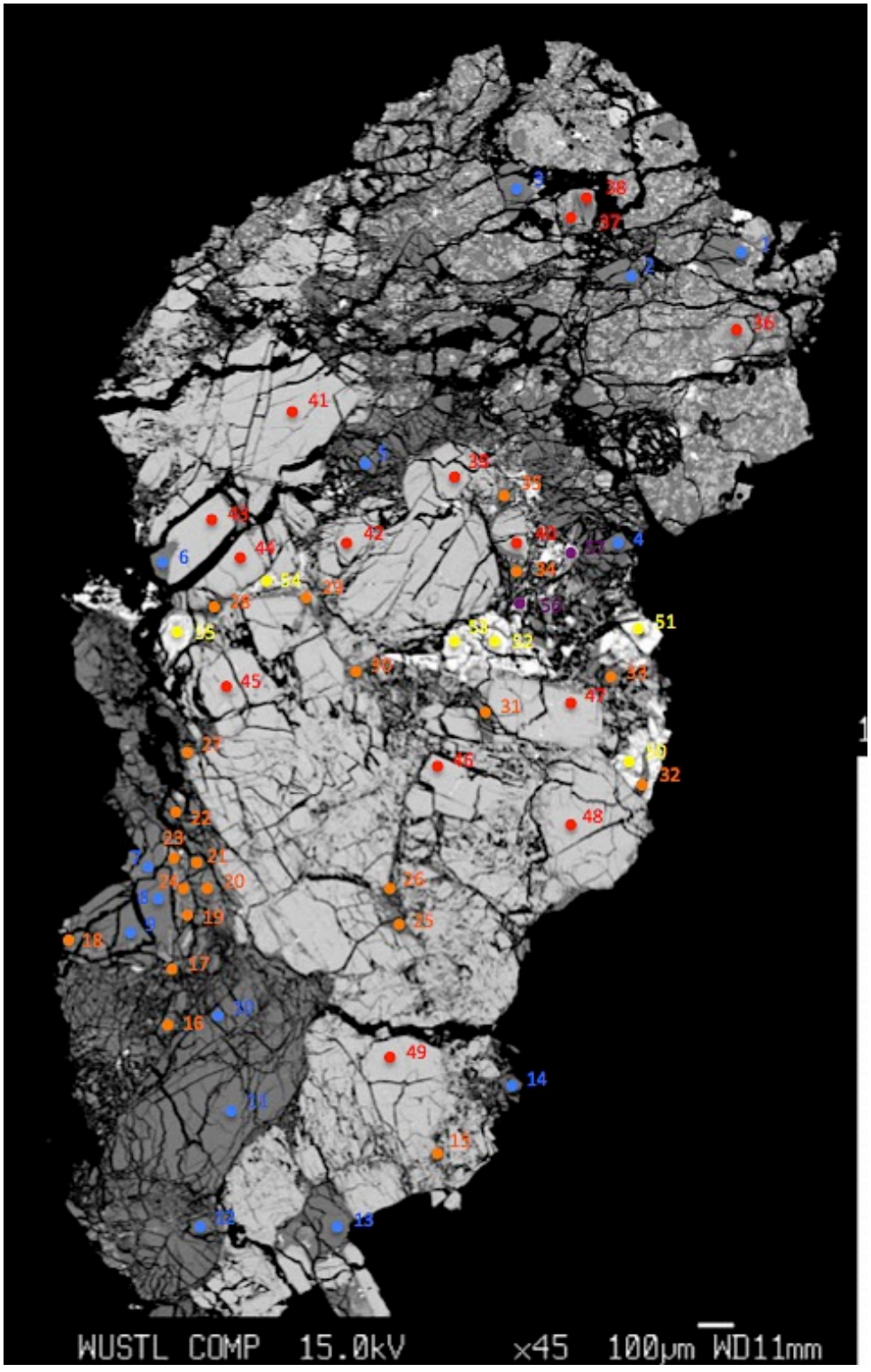

Figure A.7: EPMA map for 14304,177a. Blue dots = plagioclase, red dots = pyroxenes, orange dots = K-feldspar, and yellow dots = apatite.

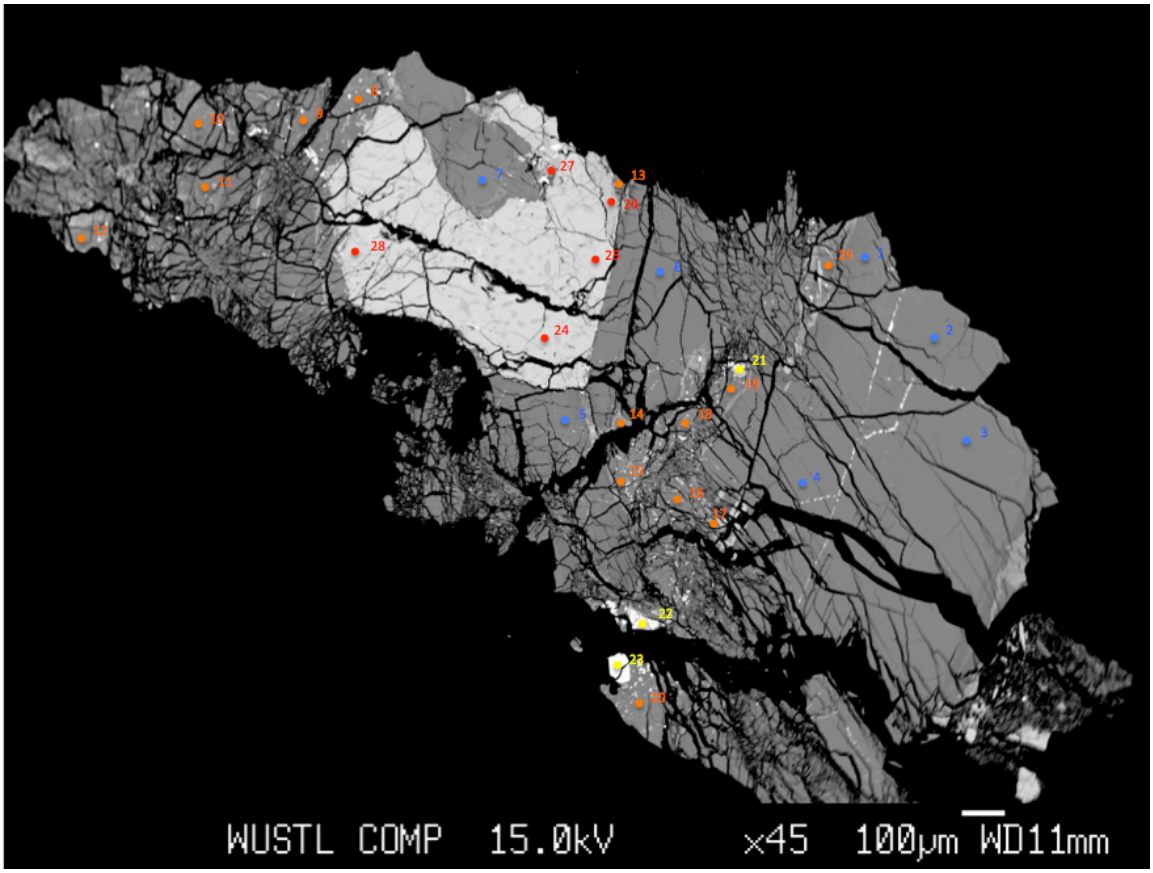

Figure A.8: EPMA map for 14304,177b. Blue dots = plagioclase, red dots = pyroxenes, orange dots = K-feldspar, and yellow dots = apatite.

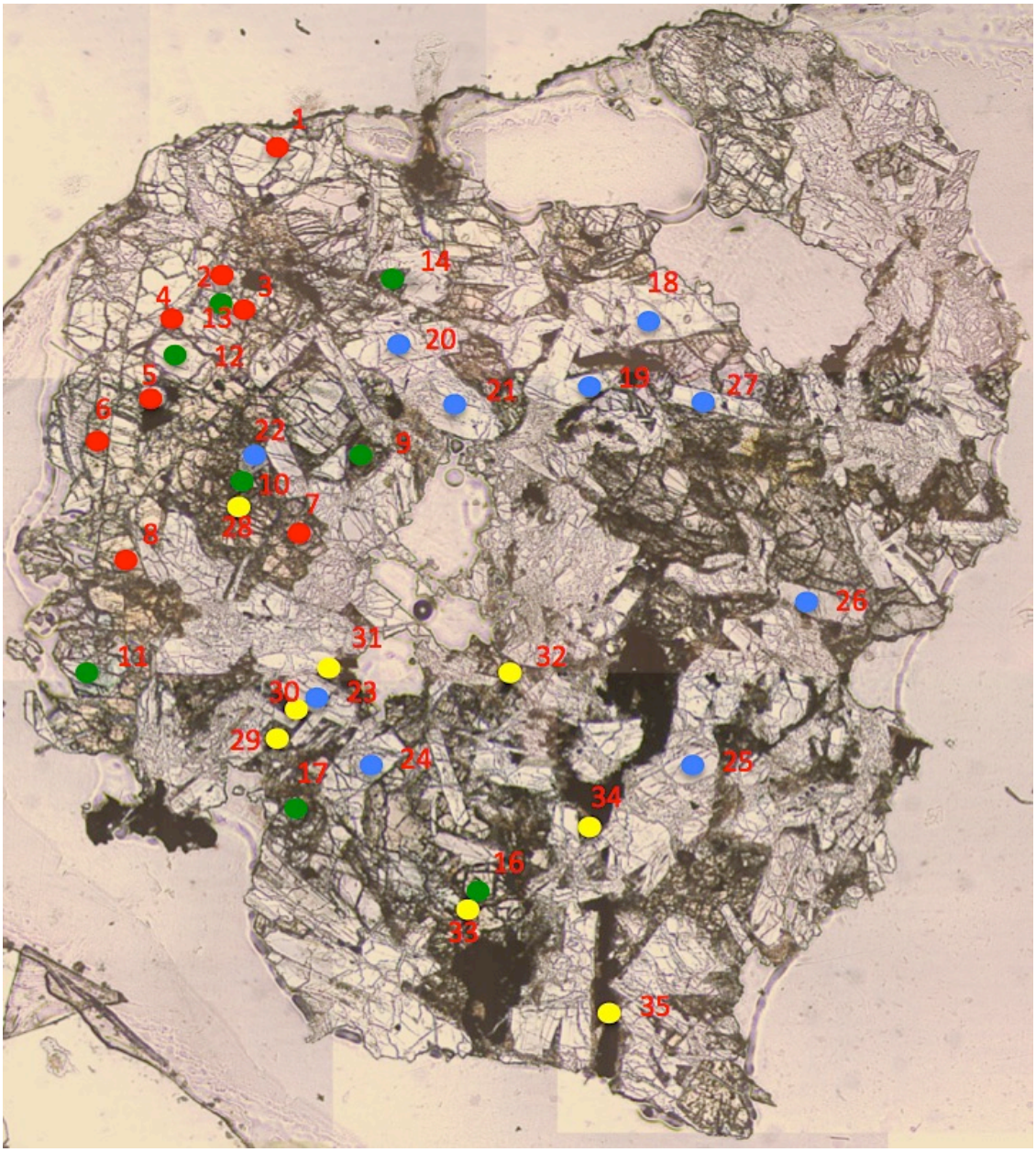

Figure A.9: EPMA map for 14304,187. Blue dots = plagioclase, red dots = pyroxenes, green dots = olivine, and yellow dots = K-feldspar.

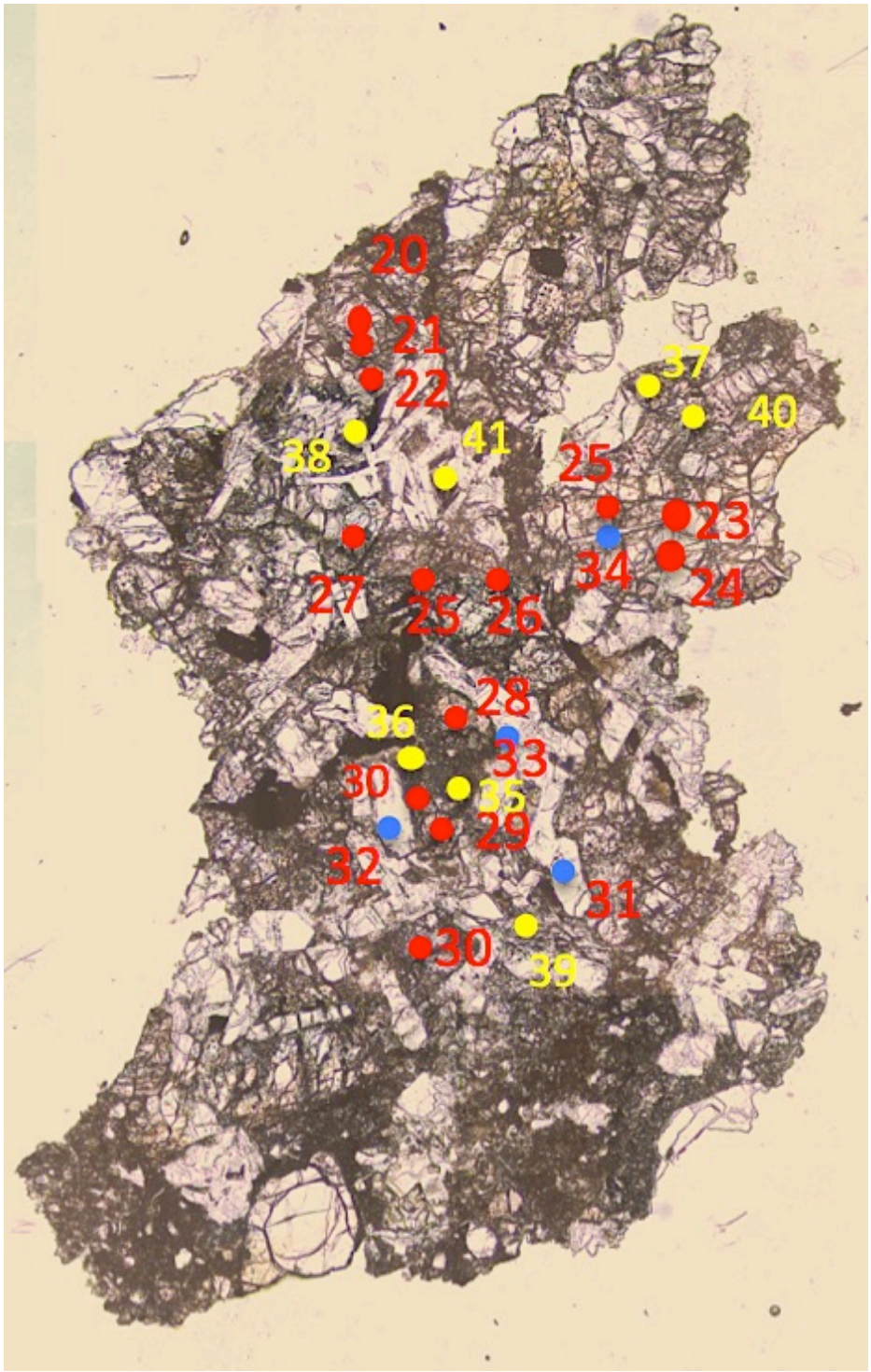

Figure A.10: EPMA map for 14304,189. Blue dots = plagioclase, red dots = pyroxenes, and yellow dots = K-feldspar.

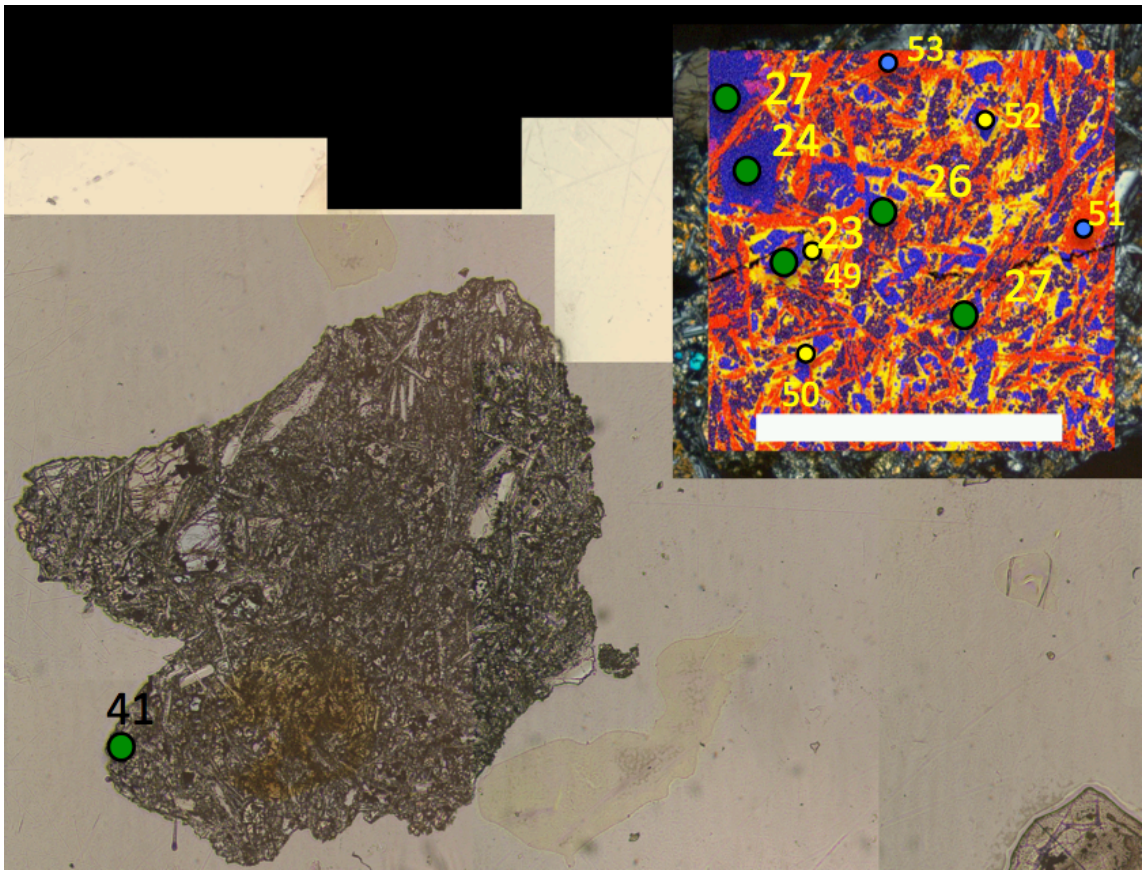

Figure A.11: EPMA map for 14304,203a. Blue dots = plagioclase, green dots = olivine, and yellow dots = K-feldspar.

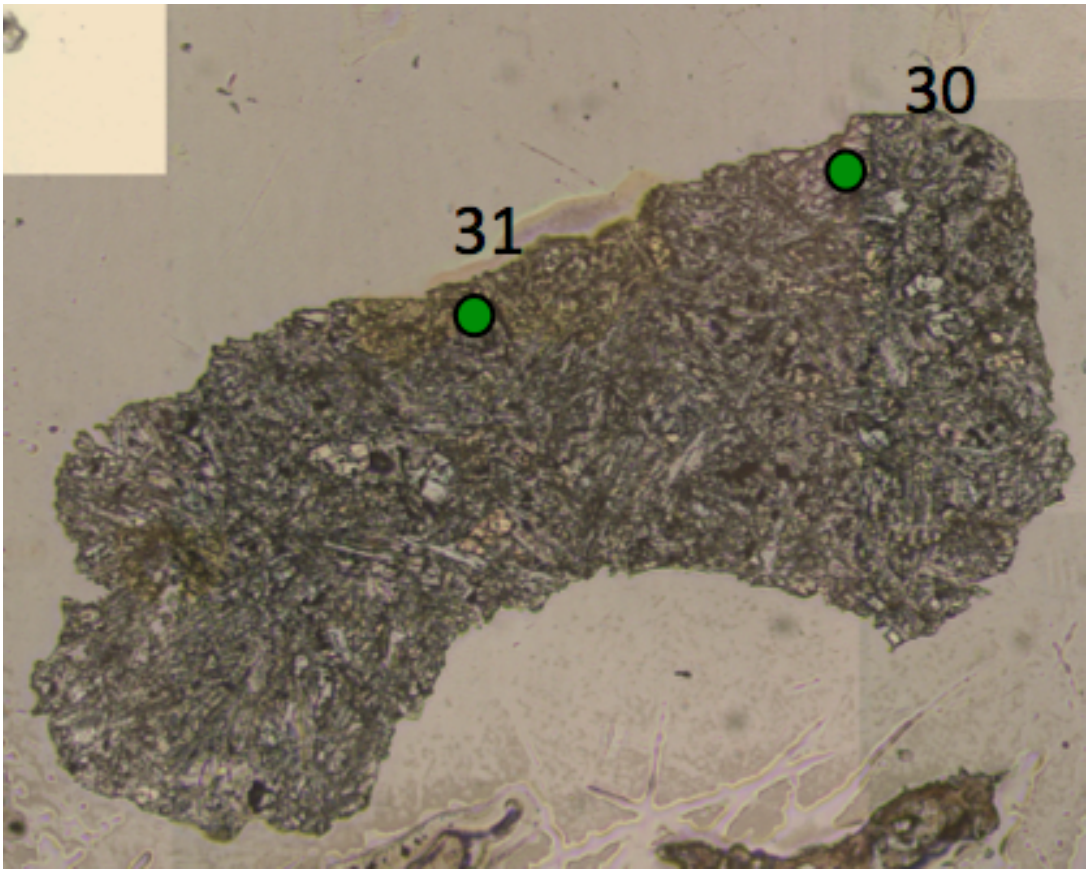

Figure A.12: EPMA map for 14304,203b. Green dots = olivine.

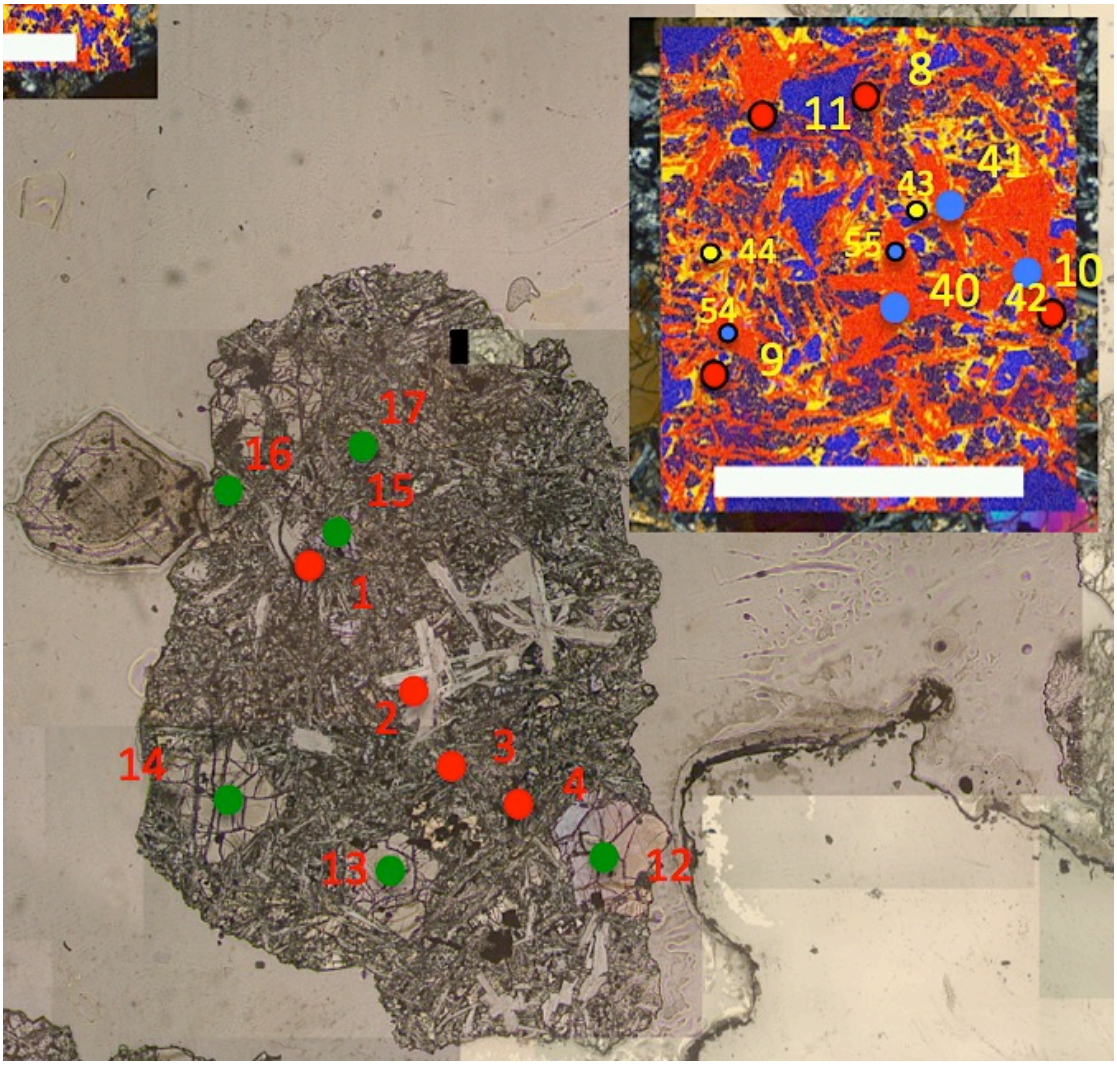

Figure A.13: EPMA map for 14304,203c. Blue dots = plagioclase, red dots = pyroxenes, green dots = olivine, and yellow dots = K-feldspar.

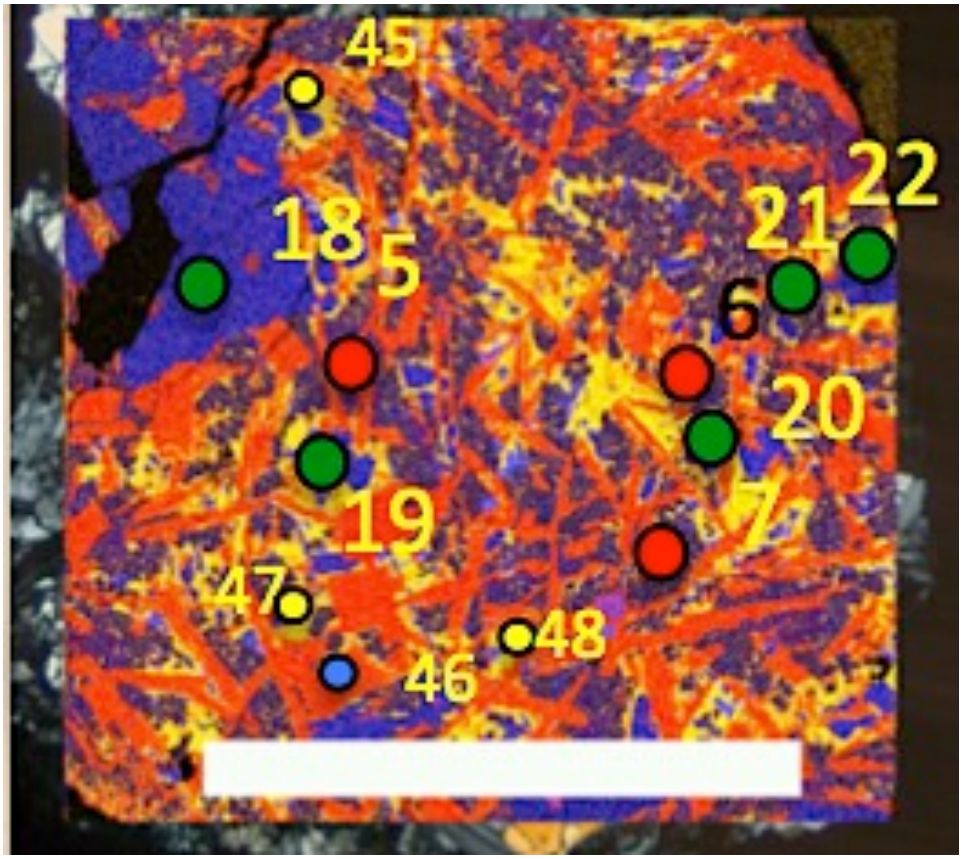

Figure A.14: EPMA map for 14304,203d. Blue dots = plagioclase, red dots = pyroxenes, green dots = olivine, and yellow dots = K-feldspar.

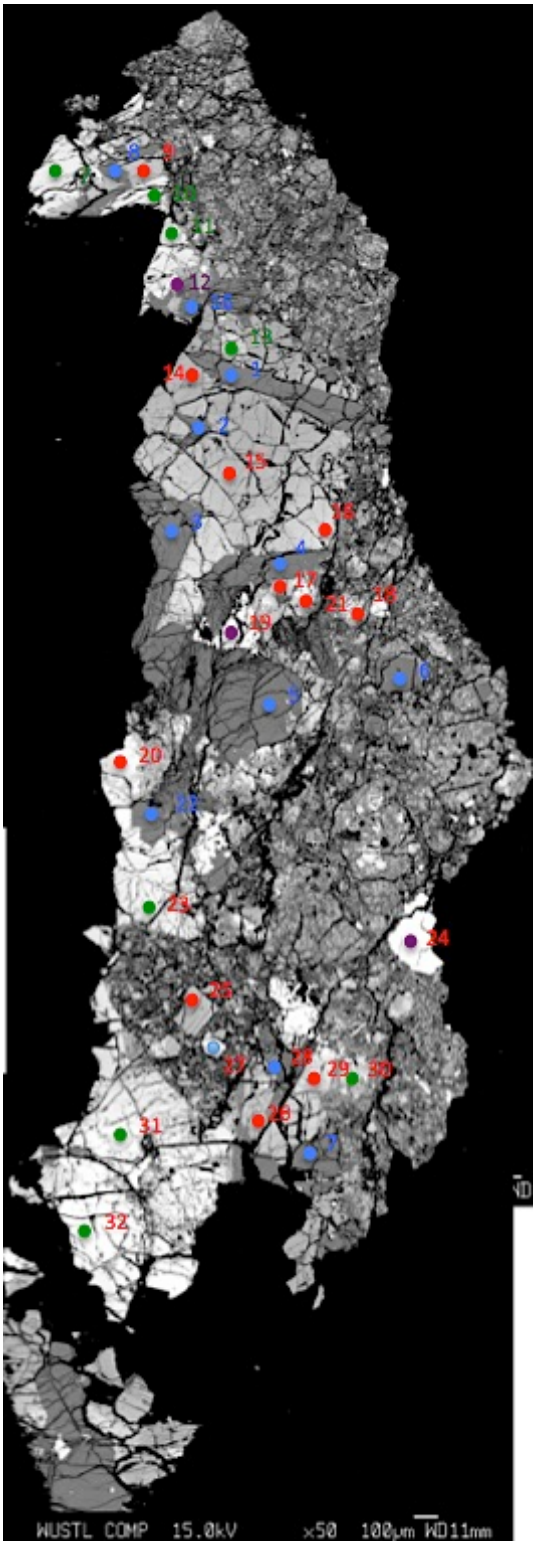

Figure A.15: EPMA map for 14304,221. Blue dots = plagioclase, red dots = pyroxenes, and green dots = olivine.

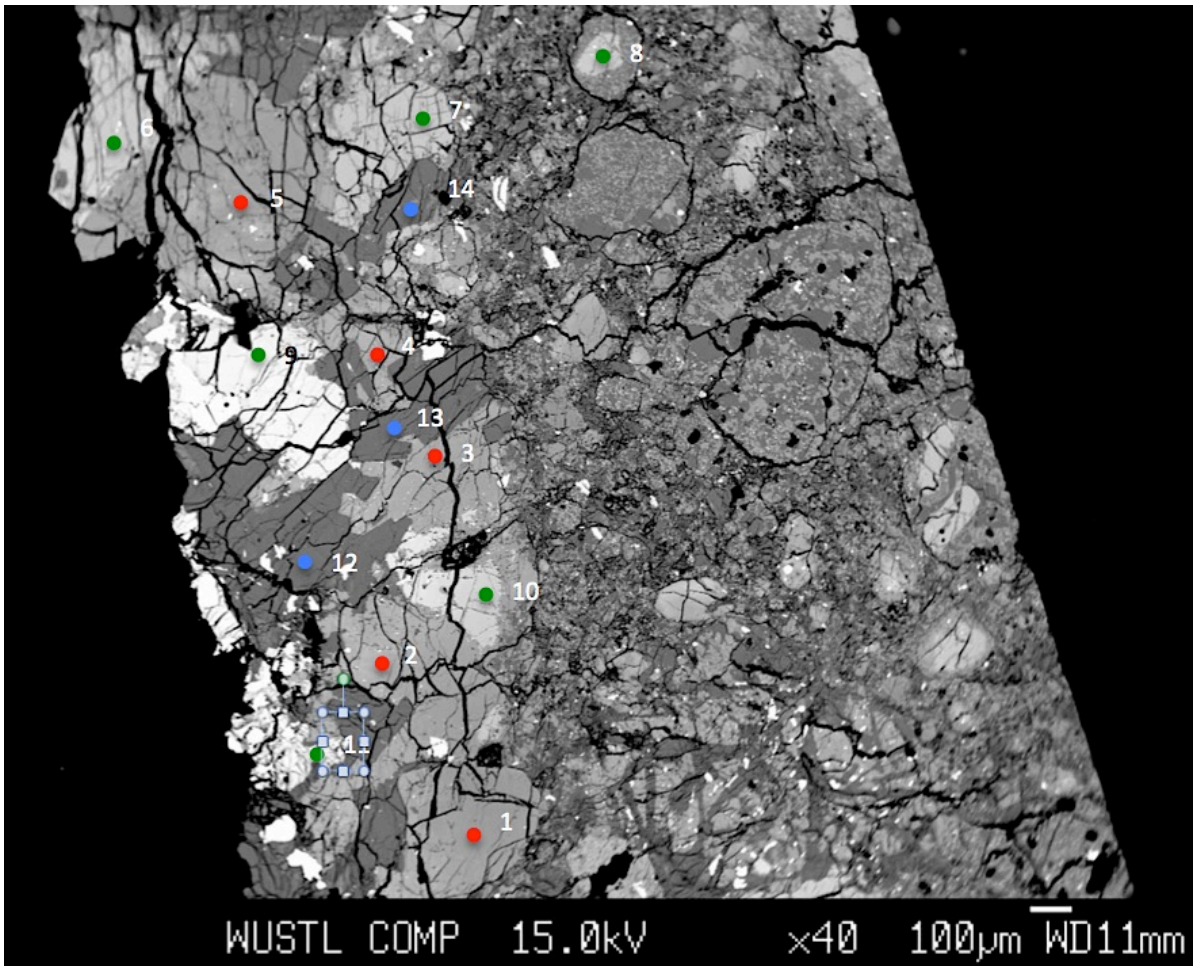

Figure A.16: EPMA map for 14304,221, thin section 299_1. Blue dots = plagioclase, red dots = pyroxenes, and green = olivine.

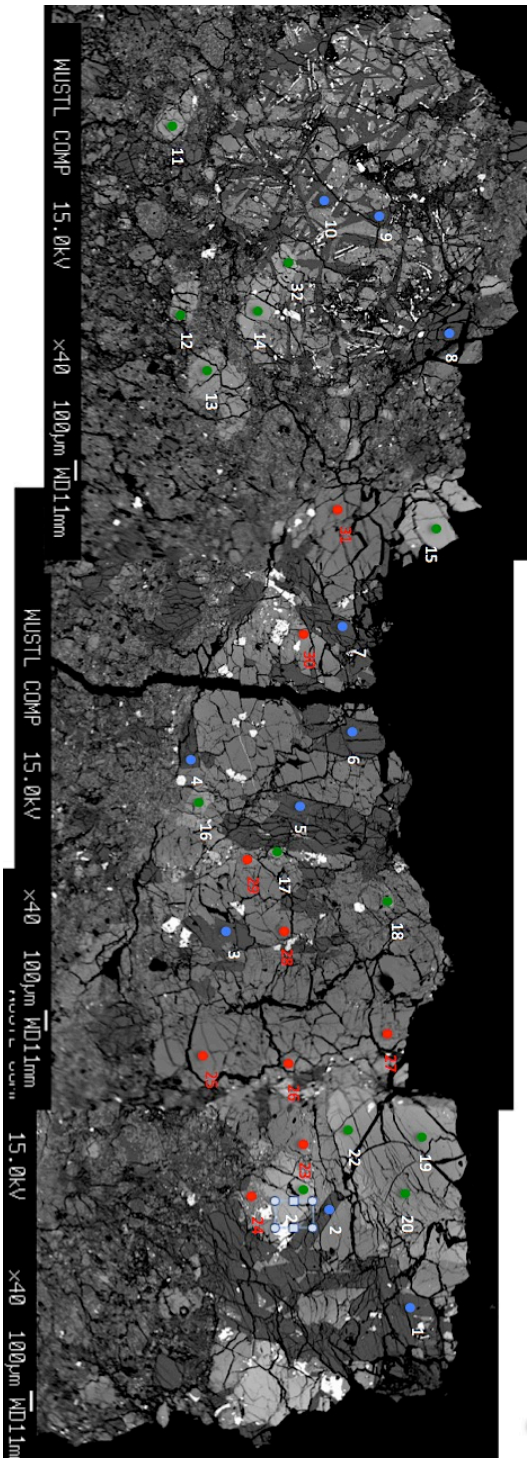

Figure A.17: EPMA map for 14304,221, thin section 299_2. Blue dots = plagioclase, red dots = pyroxenes, and green = olivine.

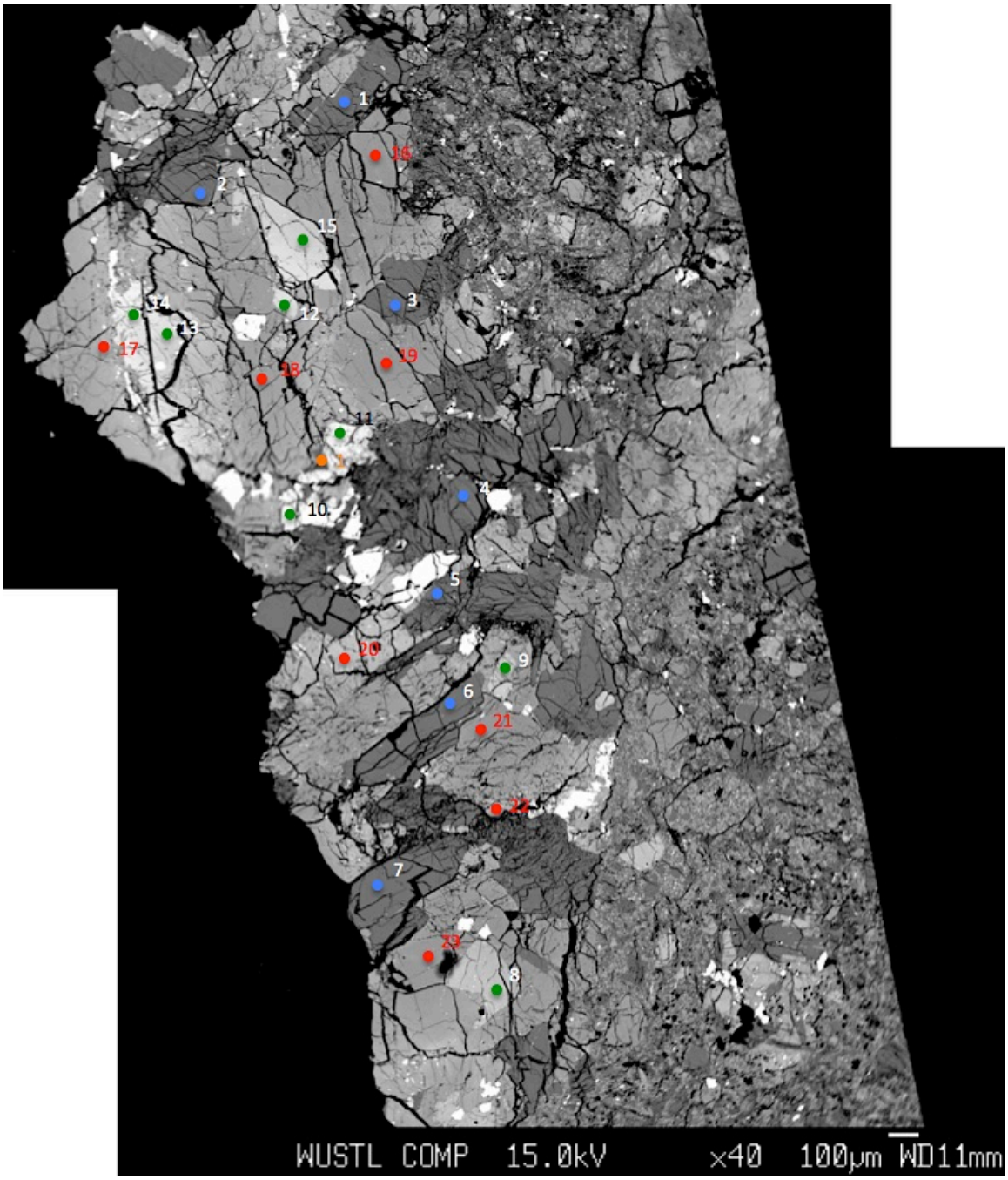

Figure A.18: EPMA map for 14304,324. Blue dots = plagioclase, red dots = pyroxenes, green dots = olivine, and orange dots = K-feldspar.

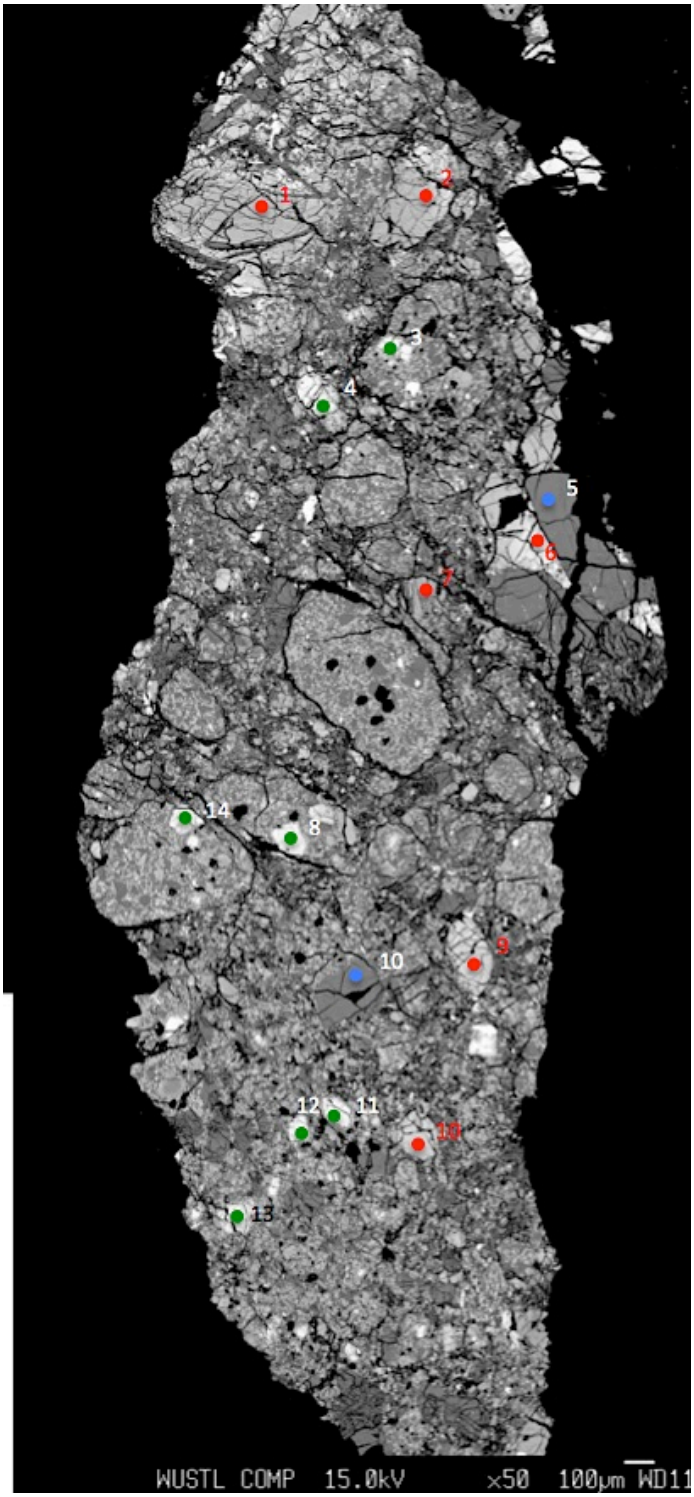

Figure A.19: EPMA map for 14304,221, thin section 326. Blue dots = plagioclase, red dots = pyroxenes, and green = olivine.

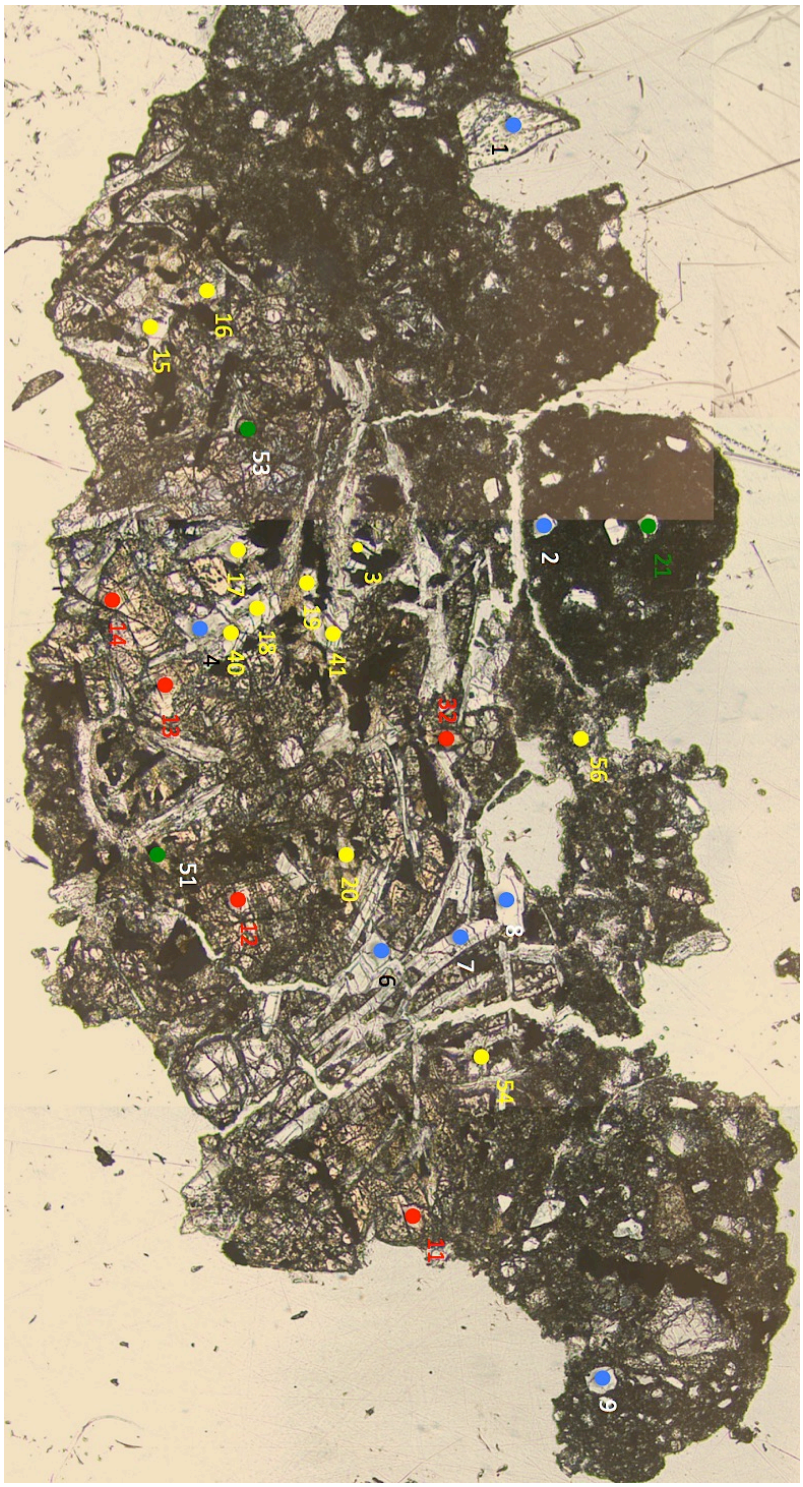

Figure A.20: EPMA map for 14305,380. Blue dots = plagioclase, red dots = pyroxenes, green dots = olivine, and yellow dots = K-feldspar.

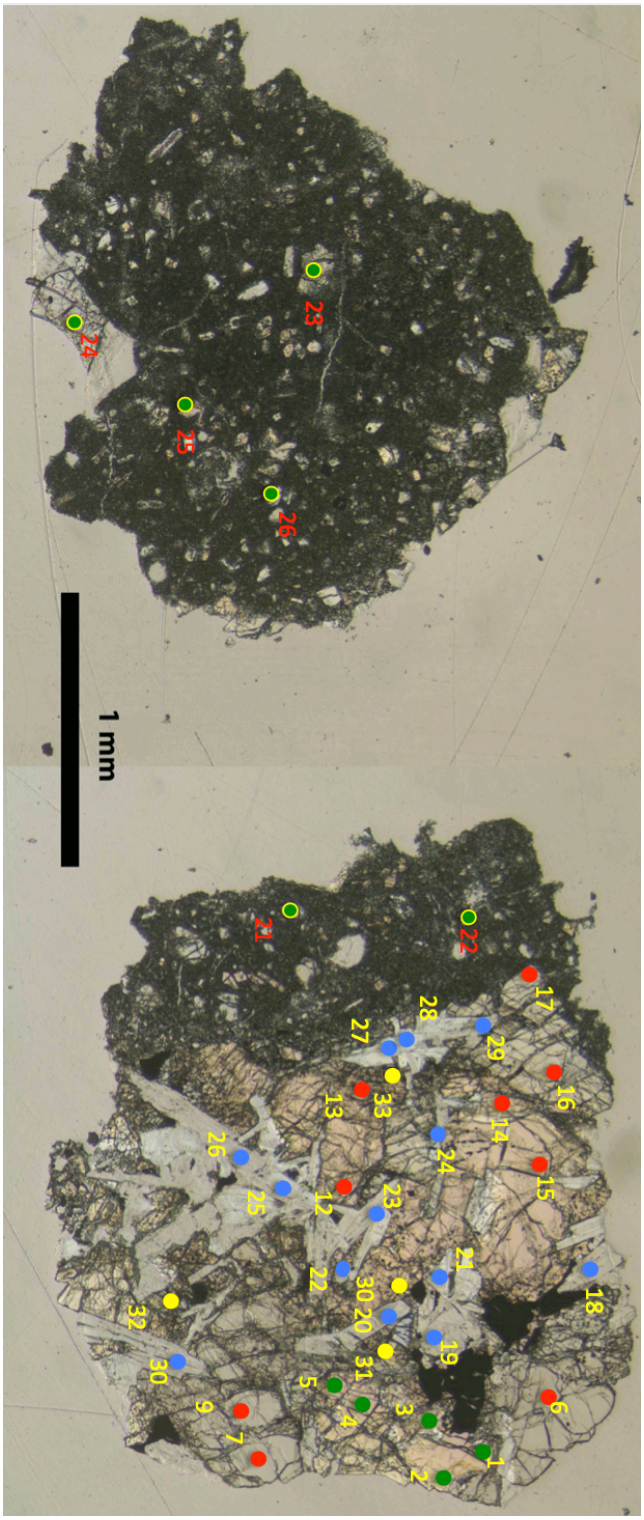

Figure A.21: EPMA map for 14305,383. Blue dots = plagioclase, red dots = pyroxenes, green dots= olivine, and yellow dots = K-feldspar.

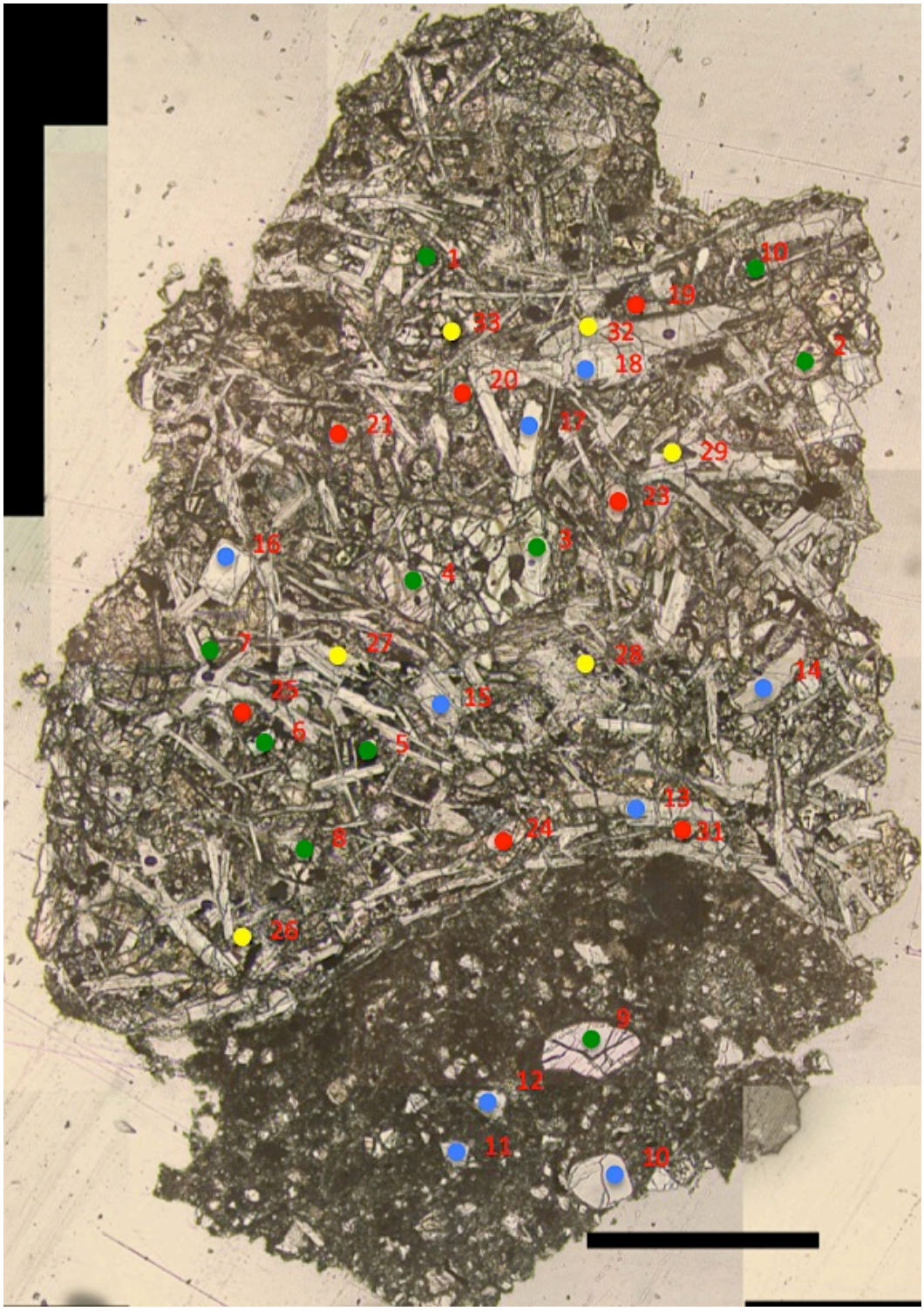

Figure A.22: EPMA map for 14305,388. Blue dots = plagioclase, red dots = pyroxenes, green dots = olivine, and yellow dots = K-feldspar.

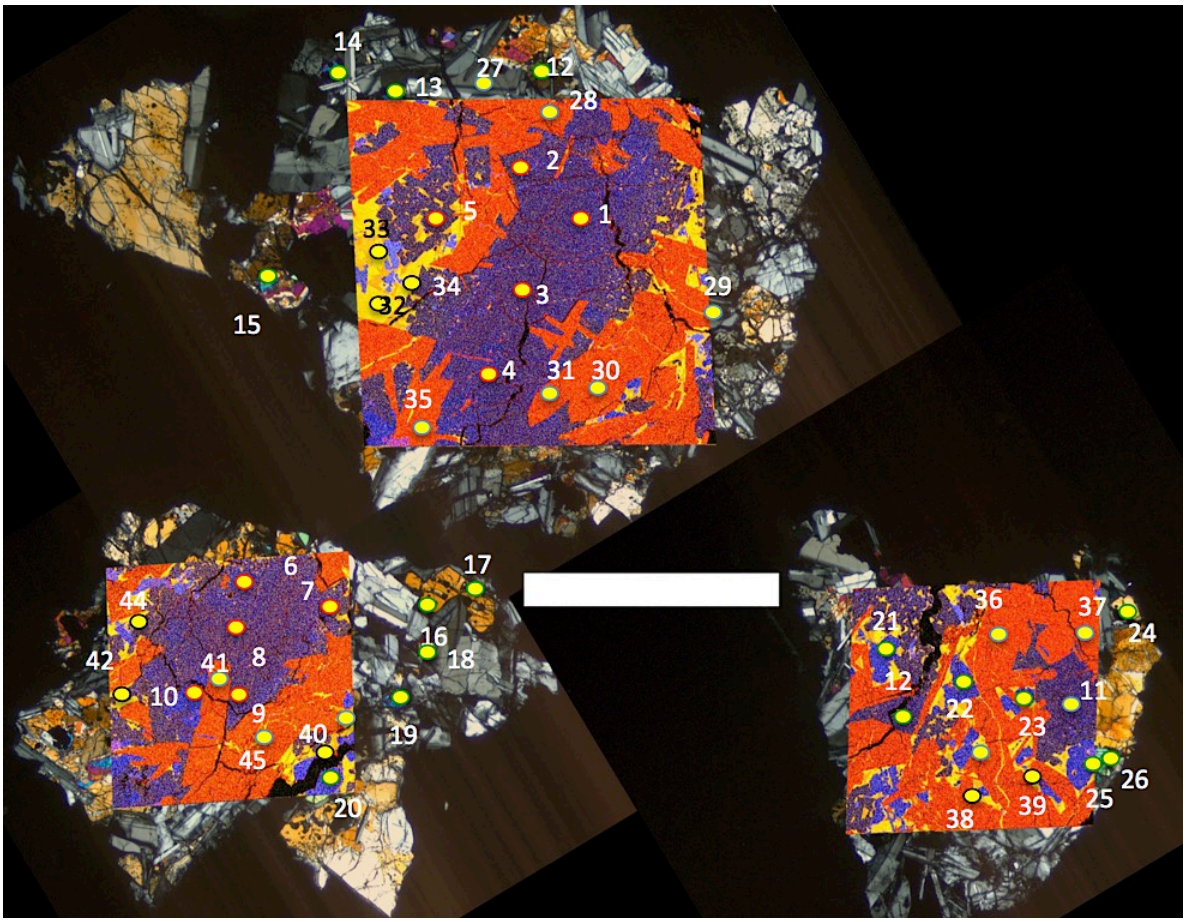

Figure A.22: EPMA map for 14305,393. Blue rimmed dots = plagioclase, red rimmed dots = pyroxenes, green rimmed dots = olivine, and yellow dots = K-feldspar.

APPENDIX B

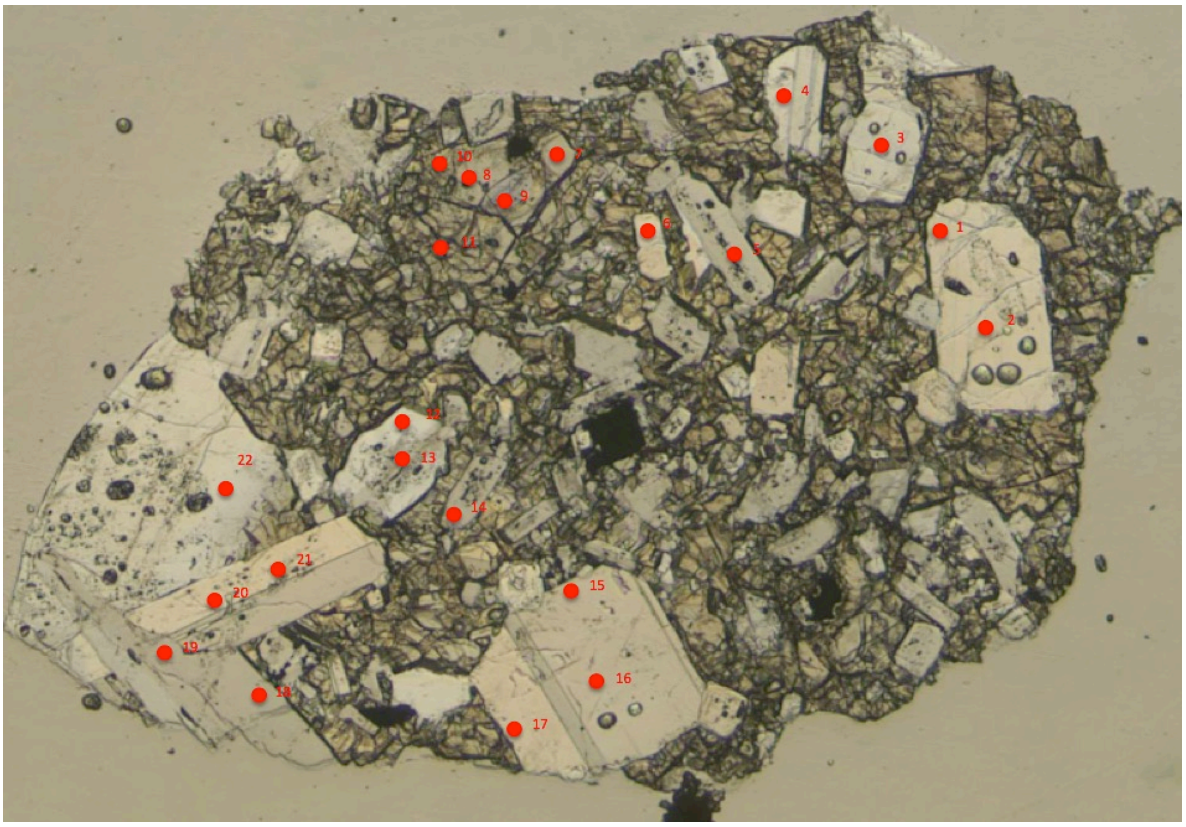

Figure B.1: LA-ICP-MS map for 14303,245.

LIST OF REFERENCES

Bindeman, I.N., and Bailey, J.C., 1999, Trace elements in anorthite megacrysts from the Kurile Island Arc: a window to across-arc geochemical variations in magma compositions: Earth and Planetary Science Letters, v. 169, p. 209-226.

Bindeman I. N., Davis A. M. and Drake M. J. ,1998, Ion microprobe study of plagioclase-basalt partition experiments at natural concentration levels of trace elements: Geochimica et Cosmochimica Acta, v 62, p. 1175–1193.

Blanchard, D.P., Jacobs, J.W., and Brannon, J.C., 1977, Chemistry of ANT-suite and felsite clasts from consortium breccia 73215 and of gabbroic anorthosite 79215: Proceedings of the 8th Lunar and Planetary Science Conference, p. 2507-2524.

Bottinga, Y., and Weill, D.F., 1970, Densities of liquid silicate systems calculated from partial molar volumes of oxide components: American Journal of Science, v. 269, p. 169-182.

Blundy J. D. and Wood B. J., 1991, Crystal-chemical controls on the partitioning of Sr and Ba between plagioclase feldspar, silicate melts, and hydrothermal solutions: Geochimica et Cosmochimica Acta, v. 55, p. 193–209.

Compston W., Vernon M.J., Berry H., Rudowski R., Gray C.M., and Ware N., 1972, Age and petrogenesis of Apollo 14 basalts: Proceedings o the 3rd Lunar and Planetary Science Conference, p. 151-153.

Depaolo, D., 1981, Trace element and isotopic effects of combined wallrock assimilation and fractional crystallization: Earth and Planetary Science Letters, v. 53, p. 189-202.

Fedele, L, Lustrino, M., Melluso, L, Morra, V., Zanetti, A, and Vannucci, R, 2015, Trace-element partitioning between plagioclase, alkali feldspar, Ti-magnetite, biotite, apatite, and evolved potassic liquids from Campi Flegrei (Southern Italy): American Mineralogist, v. 100, p. 233-249.

Giordano, D., Russell, J.K, and Dingwell, D.B., 2008, Viscosity of magmatic liquids: A model: Earth and Planetary Science Letters, v. 271, p. 123-134.

Goodrich, C.A., Taylor, G.J., Keil, K., Kallemeyn, G.W., and Warren, P.H., 1986, Alkali norite, troctolites, and VHK mare basalts from breccia 14304: Proceedings of the 16th Lunar and Planetary Science conference in Journal of Geophysical Research, v 91, p. D305-D318.

Haynes, William M., ed. (2011). *CRC Handbook of Chemistry and Physics* (92nd ed.). CRC Press. pp. 4.121–4.123. ISBN 1439855110.

Hui, H., Oshrin, J.G., and Neal, C.R., 2011, Investigation into the petrogenesis of Apollo 14 high-Al basaltic melts through crystal stratigraphy of plagioclase: Geochimica et Cosmochimica Acta, v. 75, p. 6439-6460.

Jaret, S.J., Woerner, W.R., Phillips, B.L., Ehm, L., Nekvasil, H., Wright, S.P., and Glotch, T.D., 2015, Maskelynite formation via solid-state transformation: Evidence of infrared and X-ray anisotropy: Journal of Geophysical Research, v. 120, p. 570-587.

Jolliff, B.L., Floss, C., McCallum, I.S., and Schwartz, J.M., 1999, Geochemistry, petrology, and cooling history of 14161,7373: A plutonic lunar sample with textural evidence of granitic-fraction separation by silicate-liquid immiscibility: American Mineralogist, v. 84, p. 821-837.

Kinman, W.S., and Neal, C.R., 2006, Magma evolution revealed by anorthite-rich plagioclase cumulate xenoliths from the Ontong Java Plateau: Insights into LIP magma dynamics and melt evolution: Journal of Volcanology and Geothermal Research, v. 154, p. 131-157.

Larsen, E.S., 1929, The Temperature of Magmas: American Mineralogist, v. 14, p. 81-94.

Lin, Y., Shen, W., Liu, Y., Xu, L., Hofmann, B.A., Mao, Q., Tang, G.Q., Wu, F., and Li, X.H. 2012, Very high-K KREEP-rich clasts in the impact melt breccia of the lunar

meteorite SaU 169: New constraints on the last residue of the Lunar Magma Ocean: Geochimica et Cosmochimica Acta, v., 85, p. 19-40.

Ma M.-S., Schmitt R.A., Warner R.D., Taylor G.J., Barker S., and Keil K., 1980, Aluminous mare basalts and basaltic-textured KREEPy rocks from Apollo 14 coarse fines: Proceedings of the 11th Lunar and Planetary Science Conference, p. 652-654.

Martinez, R., and Ryder, G., 1989, A granite fragment from the Appenine Front—brother of QMD?: Abstracts of the Lunar and Planetary Science Conference, v. 20, p. 620-621.

Mcdonough, W.F., and Sun, S.-s., 1995, The composition of the earth: Chemical Geology, v. 120, p. 223-253.

Neal C.R., 2001, Interior of the Moon: The presence of garnet in the primitive deep lunar mantle: Journal of Geophysical Research, v.106, p. 27865-27885.

Neal, C.R., Donohue, P., Fagan, A.L., O'Sullivan, K., Oshrin, J., and Roberts, S., (2015) Distinguishing between basalts produced by endogenic volcanism and impact processes: A non-destructive method using quantitative petrography of lunar basaltic samples: Geochemica et Cosmochimica Acta, v. 148, p. 62-80.

Neal, C.R., Taylor, L.A., and Lindstrom, M.M., 1988, The importance of lunar granite and KREEP in Very High Potassium (VHK) basalt petrogenesis: Proceedings of the 18th Lunar and Planetary Science Conference, p. 121-137.

Neal, C.R., Taylor, L.A., and Patchen, A.D., 1989a, High alumina (HA) and very high potassium (VHK) basalt clasts from Apollo 14 breccias, part 1- mineralogy and petrology: evidence of crystallization from evolving magmas: Proceedings of the 19th Lunar and Planetary Science Conference, p. 137-145.

Neal, C.R., Taylor, L.A., Schmitt, R.A., Hughes, S.S., and Lindstrom, M.M., 1989b, High alumina (HA) and very high potassium (VHK) basalt clasts from Apollo 14 breccias, part 2- whole rock geochemistry: further evidence for combined assimilation and fractional crystallization within the lunar crust: Proceedings of the 19th Lunar and Planetary Science Conference, p. 147-161.

Peckett, A., Phillips, R., and Brown, G.M., 1972, New Zirconium-rich minerals from Apollo 14 and 15 lunar rocks: Nature, v. 236, p. 215-217.

Quick, J.E., Albee, A.L., Ma, M.-S., Murali, A.V., and Schmitt, R.A., 1977, Chemical compositions and possible immiscibility of two silicate melts in 12013: Proceedings of the 8th Lunar and Planetary Science Conference, p. 2153-2189.

Roberts, S.E., and Neal, C.R., 2014a, New insights into VHK petrogenesis through quantitative textural analysis: 45th Lunar and Planetary Science Conference, abstract # 1279.

Roberts, S.E., and Neal, C.R., 2014b, Taking off the potassium coat: A new hypothesis for VHK petrogenesis: 45th Lunar and Planetary Science Conference, abstract # 1282.

Seddio, S.M., Joliff, B.L., Korotev, R.L., and Zeigler, R.A., 2013, Petrology and geochemistry of lunar granite 12032,366-19 and implications for lunar granite petrogenesis: American Mineralogist, v. 98, p. 1697-1713.

Shervais J.W., Taylor L.A., and Laul J.C., 1983, Ancient crustal components in the Fra Mauro breccias: Proceedings of the 14th Lunar and Planetary Science Conference in Journal of Geophysical Research, v. 88, p. B177-B192.

Shervais J.W., Taylor L.A., and Lindstrom, M.M., 1985a, Apollo 14 mare basalts: Petrology and geochemistry of clasts from consortium breccia 14321: Proceedings of the 16th Lunar and Planetary Science Conference, v. 90, p. C375-C395.

Shervais, J.W., Taylor, L.A., Laul, J.C., Shih C.-Y., and Nyquist, L.E., 1985b, Very high potassium (VHK) basalt: Complications in mare basalt petrogenesis: Proceedings of the 16th Lunar and Planetary Science Conference in Journal of Geophysical Research, v. 90, p. D3-D18.

Shih, C.-Y., Nyquist, L.E., Bogard, D.D., Bansal, B.M., Wiesmann, H., Johnson, P., Shervais, J.W., and Taylor, L.A., 1986, Geochronology and petrogenesis of Apollo 14 very high potassium mare basalts: Proceedings of the 16th Lunar and Planetary Science Conference in Journal of Geophysical Research, v. 91, p. D214-D228.

Stoffler, D., 1984, Glasses formed by hypervelocity impact: Journal of Non-Crystalline Solids, v. 67, p. 465-502.

Sutton, R.L., Hait, M.H., and Swann, G.A., 1972, Geology of the Apollo 14 landing site: Geochemica et Cosmochimica Acta, v. 1, p. 27-38.

Tepley, III, F. J., Lundstrom C. C., McDonough W. F. and Thompson A. (2010) Trace element partitioning between high- An plagioclase and basaltic to basaltic andesite melt at 1 atmosphere pressure: Lithos, v. 118, p. 82–94.

Warner, R.D., Taylor, G.J., Keil, K., Ma, M.-S., and Schmitt, R.A., 1980, Aluminous mare basalts: New data from Apollo 14 coarse fines: Proceedings of the 11th Lunar and Planetary Science Conference, p. 87-104.

Warren, P.H., and Wasson, J.T., 1980, Further foraging for pristine nonmare rocks: Correlations between geochemistry and longitude: Proceedings of the 11th Lunar and Planetary Science Conference, p. 431-470.

Warren, P.H., Taylor, G.J., Keil, K., Shirley, D.N., and Wasson, J.T., 1983, Petrology and chemistry of two "large" granite clasts from the Moon: Earth and Planetary Science Letters, v. 64, p. 175-185.

Warren, P.H., Shirley D.N., and Kallemeyn, G.W., 1986, A potpourri of pristine Moon rocks, inclusing a VHK mare basalt and a unique, augite-rich Apollo 17 anorthosite: Proceedings of the 16th Lunar and Planetary Science Conference In Journal of Geophysical Research, v. 91, p. 319-330.

Warren, P.H, 1993, A concise compilation of petrologic information on possibly pristine nonmare Moon rocks: American Mineralogist, v. 78, p. 360-376.

Warren, P.H., Kallemeyn G.W., and Kyte F.T., 1997, Siderophile element evidence indicates that Apollo 14 high-Al mare basalts are not impact melts: Proceedings of the 28th Lunar and Planetary Science Conference, p. 1501-1502.

Zhang Y; Evans JRG and Zhang S., 2011, "Corrected Values for Boiling Points and Enthalpies of Vaporization of Elements in Handbooks". *J. Chem. Eng. Data* **56** (2): 328–337. doi:10.1021/je1011086